

324 Material Science and Engineering Building

University of New South Wales

Kensington

Sydney

2052

2052

GFZ German Research Centre for Geosciences

Section 5.4 Hydrology

Germany

Dear Dr Blume,

I am writing on behalf of the authors of the manuscript titled "Solar forced diurnal regulation of cave drip rates via phreatophyte evapotranspiration" to thank you for your time in editing our manuscript further and for your insightful suggestions. We have responded to the recommendations point by point in the document attached and we have submitted the revised manuscript as requested. If you require any further information, please do not hesitate to contact me.

Warm regards,

Katie Coleborn

1 **Authors' response to editor's comments**

2 Dear Authors,

3

4 while the referees both see the scientific significance of this manuscript, they also both find  
5 that the scientific quality can be improved and recommend reconsideration of the  
6 manuscript after major revisions.

7 Please revise your manuscript according to their comments and suggestions.

8

9 Additionally, a few more detailed recommendations:

10 As both referees agree on the fact that the description of the methodology should be  
11 improved I also recommend adding a sketch, as suggested by referee #2.

12 We have again revised the methodology, and have now included a sketch showing the steps  
13 that were used to map and identify frequency components in the drip discharge rate,  
14 temperature and barometric pressure data. This also includes an improved outline of the  
15 advantages of synchrosqueezing over traditional signal processing methods (e.g., Fourier  
16 and wavelet transform). We hope that this satisfies both reviewers' and the editors  
17 requests.

18 Referee #1 asks whether or not the measurements of drip rates are representative, please  
19 provide a short discussion of this.

20 Thank you for raising this query. We will include a more detailed site description to address  
21 this issue:

22 "The drip sites were chosen to be representative of the cave location. We used a stratified  
23 sampling method where a transect of the cave was used to select three locations (G, M and  
24 LR) that satisfied the following criteria 1) there were actively dripping speleothems, 2)  
25 spatially distant from the other locations and 3) different depths within the cave. Individual  
26 drips were sampled randomly at each location, with selection guided by practical constraints  
27 such as the stalagmite surface being suitable for placement of a logger and the drip falling  
28 from high enough to activate pressure sensor on logger"

29

30 Referee #1 suggests showing higher resolved time series of ET and I agree that it would be  
31 helpful to show hourly or even higher resolved values instead of daily values here.

32 Thank you for your comment. We appreciate the benefit of using higher resolution ET data,  
33 however, we have used the highest resolution ET data available to us. We have used air  
34 temperature data at 15 minute intervals and have demonstrated the strong relationship  
35 between ET and temperature in the manuscript.

36

37 Referee #1 asks for an explanation of the term "negative hydraulic lift" and I am also  
38 thinking that you mistakenly mixed the two terms "hydraulic lift", which normally refers to  
39 movement of water from the roots into the soil, and "negative sapflow". Please check and  
40 clarify.

41 Thank you for bringing this point to our attention, we have amended the text in the  
42 following way:

43 “Burgess et al (2001) measured sap flow in Eucalypt tap roots, finding tap root sap flow  
44 peaked around 1 pm and negative sap flow values indicated reverse (acropetal) flow  
45 between 7pm- 7am.”

46  
47 From your responses to the specific comments #1 and #4 of referee #2 it is not clear how  
48 you intend to revise your manuscript.

49 In regards to the response to comment #1 (reviewer #2) we have added a few sentences to  
50 the introduction addressing the relevance of this manuscript along the lines of:

51 “This study has important implications for understanding karst unsaturated flow processes  
52 and karstic groundwater recharge. Currently, most karst models use very simplistic  
53 representations of unsaturated flow, if it is considered at all (Hartmann et al., 2014a). This  
54 study highlights the importance of vegetation dynamics on vadose flow and recharge  
55 making it significant to karst modelling research and speleothem-based paleoclimate studies  
56 which focus on the impact of vegetation dynamics on proxy records (Treble et al., 2015,  
57 accepted for publication 8/4/16.)”

58 Please add the recommended points to the discussion as suggested.

59 In response to comment #4 (reviewer #2) we have added the following lines to the  
60 discussion:

61 “This study clearly demonstrates the potential for vegetation to impact karst water recharge  
62 making this research relevant to karst modelling and karst water resources assessment.  
63 Currently, there are no approaches that consider the impacts of vegetation on recharge  
64 dynamics in process-based karst models (Hartmann et al., 2014b, 2015) or in empirical  
65 recharge estimation approaches (Allocca et al., 2014; Andreo et al., 2006).”

66 Please also add more quantification of the identified relationships and their significance to  
67 section 4.2.5. Solar driven daily cycles of vegetative (phreatophytic) evapotranspiration.

68 In response to the reviewer comments we have quantified the relationship between air  
69 temperature and drip rate in section 4.2.5. and have included the statistical outcome in the  
70 revised manuscript. We have provided an explanation as to why the relationship between T-  
71 amplitude/cloud cover and strength of cpd signal cannot be quantified.

72  
73 And again I would like to come back to my original suggestion of a slightly more detailed  
74 time lag analysis applying ccf or similar to all the periods with diurnal oscillations -  
75 comparing drip rates either with the temperature time series or with a time series of hourly  
76 (or 15 minute) ET. Then you would obtain a lag time and a correlation value for each of  
77 these periods (this could be presented in a plot or a table) and it would be possible to see if  
78 these values are dependent for example on the season or if they are mainly site specific.

79 Thank you for this suggestion, we have performed the cross correlation analysis for  
80 temperature and drip rate for the individual time periods where the oscillations in drip rate  
81 occur to explore how season and site explain the amount of variance in the timing of  
82 minimum drip rate. We have added Table 2 and updated the text to reflect the use of this  
83 quantitative approach:

84

85 “The daily timing of minimum and maximum drip rate varied within and between individual  
86 drip sites. At G1 the 1 cpd minimum and maximum drip rate generally appeared between  
87 12- 9 am and 3pm-12am, respectively. Daily oscillations were only observed once at G8  
88 between 14-21/05/2014 with minimum drip rate appearing 9pm and maximum drip rate  
89 appearing around 12 pm. Both 1 cpd and 2 cpd signals were observed at M10 for all the  
90 periods of drip rate oscillation with the larger peak occurring in the afternoon between 12-6  
91 pm and the smaller peak between 12-6 am, minimum drip rate appeared consistently  
92 between 6-9 am. Time lag between drip rate and air temperature was quantified by  
93 performing a cross correlation analysis with a shift interval of 15 mins up to  $\pm 24$  hours  
94 (Table 2). The lag time was identified as the point of maximum negative correlation between  
95 the two variables with the exclusion of sites with missing data. At most sites the lag time  
96 between maximum air temperature and minimum drip rate varied greatly over the  
97 monitoring period. For example, at M4 initially the lag time was 24 hours in September  
98 2013, decreasing to 9 hours in May 2014 and eventually levelling off at around 16 hours  
99 from September to December 2014. In contrast, G1 had a similar lag time over all 4 periods  
100 of drip rate fluctuation ranging from from 11.25- 12.75 hours. G6 was unique in that the  
101 minimum drip rate occurred before the maximum air temperature in February and March  
102 2013, January 2014 and 2015. Analysis of variance indicated that drip site and season did  
103 not explain a significant amount of variance in lag time.”

104 “Across all sites, lag time between maximum air temperature and minimum drip rate can  
105 range from 0.25- 24 hours (Table 2). We can hypothesise that those sites with a shorter lag  
106 time have a shorter path length from tree root accessed store to cave discharge site than  
107 the other drip sites. For example, the lag time for site G1 ranges from 11.25-12.75 hours  
108 whereas site G10 ranges from 0.5- 3 hours. This process could also explain the large  
109 variation in lag time within a particular site, for example at G6 the lag time was 21 hours in  
110 May 2014 and decreased to 7 hours in August 2014 (Table 2).”

111 “Conversely, we can hypothesise that G6 has a small store volume that is more sensitive to  
112 water uptake by tree roots, which is why we see the minimum drip rate occurring 0.25-7  
113 hours before peak air temperature (Table 2).”

114

115

116 Looking forward to your revised manuscript,

117 Theresa Blume

1 **Solar forced diurnal regulation of cave drip rates via phreatophyte evapotranspiration**

2

3 Katie Coleborn<sup>1</sup>, Gabriel C. Rau<sup>1</sup>, Mark O. Cuthbert<sup>2</sup>, Andy Baker<sup>1</sup>, Owen Navarre<sup>3</sup>

4 <sup>1</sup>*Connected Waters Initiative Research Centre, UNSW Australia, Kensington, NSW 2052*  
5 *Australia*

6 <sup>2</sup>*School of Geography, Earth and Environmental Sciences, University of Birmingham,*  
7 *Edgbaston, Birmingham, B15 2TT, UK*

8 <sup>3</sup>*School of Biology Earth and Environmental Sciences, UNSW Australia, Kensington, NSW*  
9 *2052 Australia*

10

11 Corresponding author: Katie Coleborn

12 Email: [k.coleborn@unsw.edu.au](mailto:k.coleborn@unsw.edu.au)

13 Tel: +61434105636

## 14 Abstract

15 We present results of a detailed study of drip rate variations at 12 drip discharge sites in  
16 Glory Hole Cave, New South Wales, Australia. Our novel time series analysis, using the  
17 synchrosqueeze transform, reveals pronounced oscillations at daily and sub-daily  
18 frequencies occurring in 8 out of the 12 monitored sites. These oscillations were not  
19 spatially or temporally homogenous, with different drip sites exhibiting such behaviour at  
20 different times of year in different parts of the cave. We test several hypotheses for the  
21 cause of the oscillations including variations in pressure gradients between karst and cave  
22 due to cave breathing effects or atmospheric and earth tides, variations in hydraulic  
23 conductivity due to changes in viscosity of water with daily temperature oscillations, and  
24 solar driven daily cycles of vegetative (phreatophytic) transpiration. We conclude that the  
25 only hypothesis consistent with the data and hydrologic theory is that daily oscillations are  
26 caused by solar driven pumping by phreatophytic trees which are abundant at the site. The  
27 daily oscillations are not continuous and occur sporadically in short bursts (2-14 days)  
28 throughout the year due to non-linear modification of the solar signal via complex karst  
29 architecture. This is the first observation of tree water use in cave drip water and has  
30 important implications for karst hydrology in regards to developing a new protocol to  
31 determine the relative importance of trends in drip rate, **such as diurnal oscillations, at**  
32 **different timescales and how these trends change over timescales of weeks to years. This**  
33 **information can be used ~~and~~ to infer karst architecture. This study also demonstrates the**  
34 **importance of vegetation on recharge dynamics, information that will inform both process-**  
35 **based karst models and empirical estimation approaches.** Our findings support a growing  
36 body of research exploring the impact of trees on speleothem paleoclimate proxies.

## 37 1. Introduction

38 Karst architecture determines the flow and storage of water from the surface to the  
39 underlying cave and is a major influence on drip discharge. Karst systems are characterised  
40 by three principle flow types. Primary flow occurs where the water travels through the  
41 primary porosity of the rock matrix, secondary flow pathways are characterised by water  
42 transported along fractures in the bedrock and tertiary flow pathways consist of conduits  
43 enlarged by dissolution. **The dominance of a particular flow regime changes over time, for**  
44 **example, older limestone tends to have higher secondary porosity (more fractures and**  
45 **enlarged conduits) and a lower primary porosity due to compaction or cementation (Ford**  
46 **and Williams, 1994). ~~The dominance of a particular flow regime can be influenced by the~~**  
47 **age of the limestone, for example, older limestone tends to be more heavily karstified (more**  
48 **fractures and enlarged conduits) with a lower primary porosity due to marmorisation.** The  
49 relationship between karst architecture and delivery of water to cave drip discharge sites  
50 has been studied to constrain uncertainty in paleoclimate studies (Bradley et al., 2010;  
51 Markowska et al., 2015), identify suitable speleothems as climate archives (McDonald and  
52 Drysdale, 2007) and in conjunction with drip water geochemistry to determine water

53 residence times in karst aquifers ([Arbel et al., 2010](#); [Fairchild et al., 2000](#); [Lange et al., 2010](#);  
54 [Sheffer et al., 2011](#); [Tooth and Fairchild, 2003](#); [Treble et al., 2013b](#)). Recent research ~~into~~  
55 [examining](#) drip hydrology and fluctuations in drip rate have used hydrological response to  
56 characterise flow paths. For example, Markowska et al., (2015) used statistical analysis of  
57 drip hydrology data to identify storage flow, in both the epikarst and overlying soil, to  
58 develop conceptual models of a karst system.

59 Over a timescale of months to years, fluctuations in drip discharge are typically driven by  
60 seasonal variation in water availability (Hu et al., 2008; Sondag et al., 2003) and long-term  
61 climate forcings such as the North Atlantic Oscillation or El Niño-Southern Oscillation  
62 (McDonald, 2004; Proctor et al., 2000). On a daily to weekly timescale, drip rate responds to  
63 individual rainfall events (Baldini et al., 2012) and barometric changes (Genty and Deflandre,  
64 1998; Jex et al., 2012; Tremaine and Froelich, 2013). Tremaine and Froelich (2013) found  
65 weekly and daily fluctuations at one drip site where an increase in barometric pressure  
66 decreased volumetric drip rate. This was attributed to atmospheric tides, the heating and  
67 cooling of the atmosphere, as the diurnal cycles occurred at two hours before the solar  
68 noon (S1) and solar midnight (S2) each day. The cave was situated in poorly to moderately  
69 indurated Oligocene limestone with a high likelihood of primary porosity (Scott, 2001). Jex  
70 et al. (2012) observed a negative correlation between weekly barometric pressure changes  
71 and drip rate at two out of forty drip sites monitored at the base of a paleokarst feature in  
72 the marmorised and fractured Devonian limestone at Cathedral Cave, NSW. One drip  
73 discharge site had a relatively strong anti-correlation ( $R=-0.52$ ) after accounting for a 40 hr  
74 time lag. This relationship was attributed to a two-phase flow, where pressure fluctuations  
75 expanded and compressed air bubbles in the water held within the paleokarst in the  
76 unsaturated zone.

77 Non-linear and chaotic behaviour of drip discharge has been observed over very short  
78 (second to minutes) timescales. Chaotic drip regimes were first noted by Genty and  
79 Deflandre (1998) in the Devonian limestone of southern Belgium (Genty and Deflandre,  
80 1998). Chaotic and non-linear drip responses were also observed at an event-scale in the  
81 fractured-rock limestone of Cathedral Cave, NSW (Mariethoz et al., 2012). These were  
82 attributed to the filling and draining of subsurface karst stores within a recharge event, with  
83 increasing homogenisation of flow with the filling of the stores. Baker and Brunson (2003)  
84 observed non-linear responses to rainfall in multi-year drip time series from a fractured rock  
85 (Carboniferous limestone) in Yorkshire, UK. With the exception of Tremaine and Froelich  
86 (2013), daily fluctuations have not been observed in cave drip water hydrology. In this paper  
87 we aim to increase our understanding of karst architecture by using a novel approach, the  
88 synchrosqueeze transform, to analyse drip discharge time series from 12 drip discharge sites  
89 in Glory Hole Cave, SE Australia. This analysis allows us to characterise daily and sub-daily  
90 fluctuations in drip rate and identify the processes driving these oscillations. **This study has**  
91 **important implications for understanding karst unsaturated flow processes and karstic**  
92 **groundwater recharge. Currently, most karst models use very simplistic representations of**

93 unsaturated flow, if it is considered at all (Hartmann et al., 2014a). This study highlights the  
94 importance of vegetation dynamics on vadose flow and recharge making it significant to  
95 karst modelling research and speleothem-based paleoclimate studies which focus on the  
96 impact of vegetation dynamics on proxy records (Treble et al., 2015, ~~n.d2016~~.)

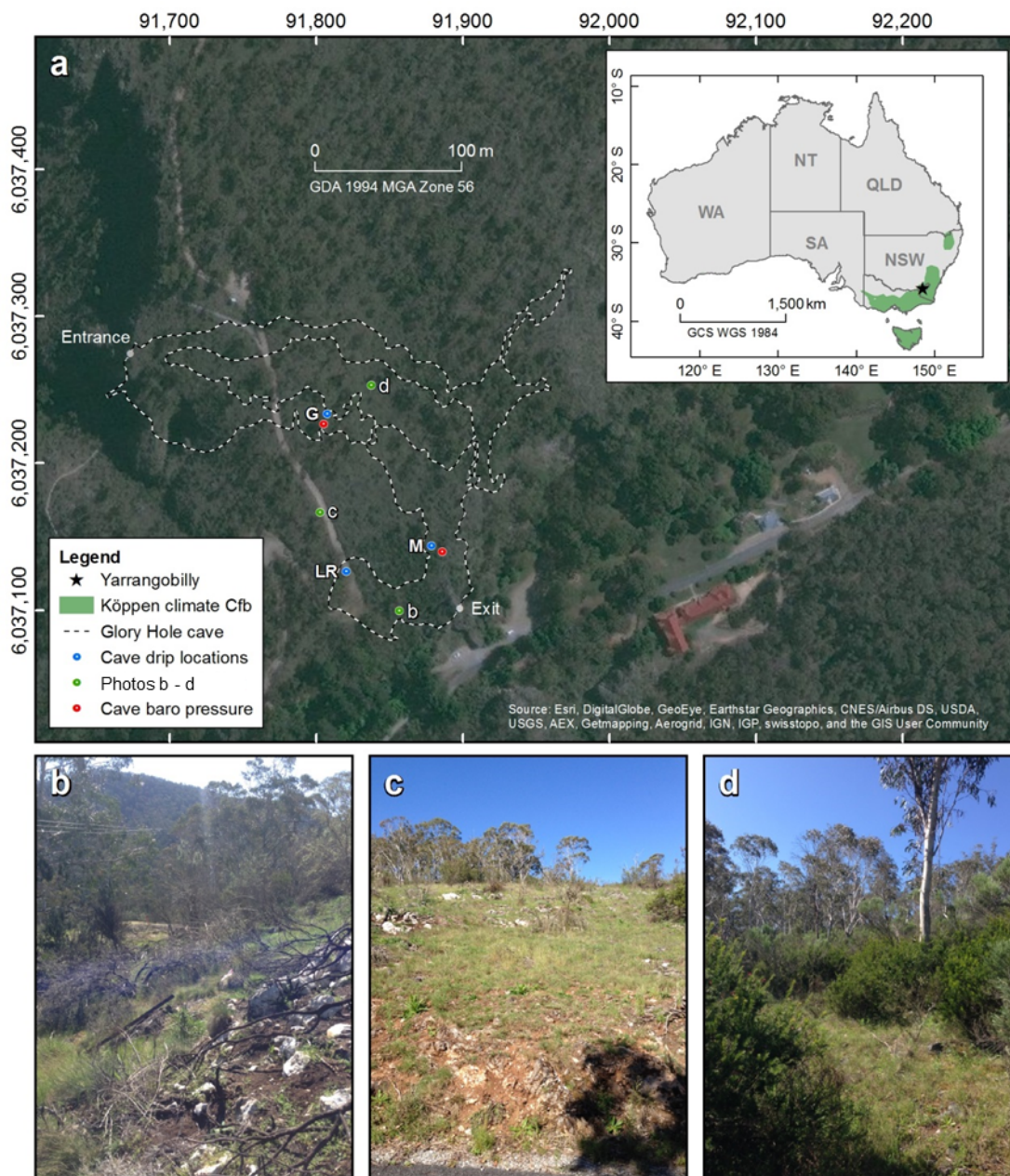
97



98 **2. Field site and methods**

99 **2.1 Glory Hole Cave at Yarrangobilly Caves National Park**

100 Glory Hole Cave is part of the Yarrangobilly Caves National Park located in the Snowy  
101 Mountains, New South Wales, Australia (35°43'29.3"S 148°29'14.9"E) at an elevation of 980  
102 m (Australian Height Datum)AHD. The Snowy Mountains forms part of the Great Dividing  
103 Range, a mountainous region stretching along the eastern seaboard from Queensland to  
104 Victoria. The region is sub-alpine and the climate is classified as temperate montane with  
105 mild summers and no dry season (Köppen climate classification Cfb) (Peel et al., 2007; Stern  
106 et al., 2012).



107

108 Figure 1 location of Yarrangobilly Caves in New South Wales, Australia with photos of  
109 surface vegetation b-d. Extent of Köppen climate zone is from Peel et al. (2007).

110 Glory Hole Cave is formed of two main sections connected by a narrow constriction ~2 m x 6  
111 m. It is ~243 m in length and is ~100 m at its widest point. The cave extends more than 40 m  
112 below the surface in an unsaturated zone of westward sloping limestone bedrock **with a**  
113 **contributing catchment area of ~1 km<sup>2</sup>**. The cave is situated within a formation of massive  
114 limestone approximately 12 km long and on average 1 km wide (Worboys, 1982). The  
115 limestone is typical of south-eastern Australian limestone; it is Silurian, highly fractured and  
116 marblised with little primary porosity. The bedding planes of the limestone are generally  
117 obvious with a westward dip (Adamson and Loudon, 1966). It is likely that Glory Hole Cave  
118 was formed by water running off less permeable rocks to the east of the limestone, sinking  
119 to the water table and rising through large springs close to the Yarrangobilly River (Spate,  
120 2002) which is situated in a gorge in <100 m west of the cave entrance. **Glory Hole Cave is**  
121 **likely to be relevant for paleoclimate proxies as it is well decorated and in close proximity**  
122 **(<100 m) to caves that have been used in multi-proxy speleothem based paleoclimate**  
123 **studies (Markowska et al., 2015; Webb et al., 2014).**

124 The vegetation is classified as sub-alpine open snowgum (*Eucalyptus pauciflora* subsp.  
125 *pauciflora*) and black sallee (*E. stelullata*) woodland.

126

## 127 **2.2 Cave and surface monitoring**

128 Drip discharge rate was recorded at 12 drip sites in three locations (Fig. 1 and Table 1)  
129 within Glory Hole Cave using Stalagmate© drip loggers between December 2012 and  
130 September 2015, and monitoring is ongoing. **The drip sites were chosen using a stratified**  
131 **sampling method. A transect of the cave was used to select three locations (G, M and LR)**  
132 **that satisfied the following criteria 1) there were actively dripping speleothems, 2) spatially**  
133 **distant from the other locations and 3) different depths within the cave. Individual drips**  
134 **were sampled randomly at each location, with selection guided by practical constraints such**  
135 **as stalagmite surface being suitable for placement of logger and the drip falling from high**  
136 **enough to activate pressure sensor on the logger.** Drip loggers recorded the frequency of  
137 drips falling onto the surface of the sealed box containing an acoustic sensor in 15 min  
138 intervals. The number of drips were converted to ml min<sup>-1</sup>, assuming that 1 drip equals 0.19  
139 ml (Collister and Matthey, 2008; Markowska et al., 2015). Recently, automated drip loggers  
140 have been widely used in cave hydrology research (Cuthbert et al., 2014b; Hu et al., 2008;  
141 Mahmud et al., 2015; Rutledge et al., 2014; Treble et al., 2013a) as they provide a more  
142 convenient and efficient way of recording higher temporal resolution data than traditional  
143 drip counting methods.

144

145 Table 1 Summary of drip sites and location within cave as indicated in Fig. 1, the mean and  
 146 standard deviation (std) of total flow volume and maximum and minimum drip rate in  
 147 summer (December- February) and winter (June- August).

Site	Location	Total flow volume (L)				Drip rate (ml min <sup>-1</sup> )			
		Summer		Winter		Summer		Winter	
		mean	std	mean	std	Maximum	Minimum	Maximum	Minimum
G1	G	72.67	9.21	209.58	107.78	19.51	1.84	56.75	0.00
G3		23.76	10.13	115.44	8.37	7.00	0.00	34.43	0.00
G6		3.73	1.90	16.45	0.10	1.43	0.10	4.10	0.65
G8		6.36	0.49	5.81	0.16	1.11	0.00	0.96	0.34
G10		32.47	23.08	104.54	73.58	9.97	0.04	27.27	0.00
G12		6.57	5.71	9.74	4.39	1.68	0.00	2.04	0.43
LR1	LR	32.31	23.93	98.62	7.39	58.30	0.00	57.77	0.00
M1	M	0.29	0.18	0.47	0.00	0.13	0.00	0.11	0.00
M2		7.67	12.85	120.09	21.21	42.53	0.00	74.30	0.00
M4		0.88	1.47	33.95	5.17	4.02	0.00	28.45	0.00
M10		24.53	34.68	127.79	51.36	13.95	0.00	27.56	0.00
M13		7.33	5.05	67.03	6.60	12.40	0.09	41.80	0.92

148

149 Barometric pressure and air temperature were recorded at two locations within the cave  
 150 (Fig. 1) using Solinst level loggers at 15 min intervals from January-September 2015.  
 151 Precipitation (accuracy  $\pm 4\%$  of total mm), wind speed (accuracy  $\pm 0.1$  kph), relative  
 152 humidity (accuracy  $\pm 2\%$ ), air temperature (accuracy  $\pm 0.5$  °C) and barometric pressure  
 153 (accuracy:  $\pm 1.0$  kPa/mb) were measured with a Davis Vantage Pro 2 weather station <1 km  
 154 from Glory Hole Cave at 15 min intervals and data stored using a Datalogger DT80 data  
 155 logger. Solar radiation ( $\text{MJ m}^{-2}$ ) was derived from satellite imagery processed by the Bureau  
 156 of Meteorology from the Geostationary Meteorological Satellite and MTSAT series.

157 Daily potential evapotranspiration was estimated using ETo Calculator software developed  
 158 by the Land and Water Division of the Food and Agriculture Organisation of the United  
 159 Nations <http://www.fao.org/nr/water/eto.html>. The software is based on the Penman-  
 160 Monteith equation and is a physically-based method with physiological and aerodynamic  
 161 parameters. The climate parameters used were air temperature (mean, maximum and  
 162 minimum), relative humidity (mean, maximum and minimum), wind speed and solar  
 163 radiation.

164

### 165 2.3 Spectral analysis of cave drip discharge rates

166 A new advance in signal processing was used to analyse the frequency-time content of  
 167 measured cave drip discharge rate, temperature and barometric pressure. Daubechies et al  
 168 (2011) first presented the synchrosqueeze transform (SST) as an empirical mode

169 decomposition like tool for disentangling a complex signal into approximately harmonic  
 170 components Thakur et al (2013) adapted the SST to discretised data (rather than continuous  
 171 functions) and developed a MATLAB Synchrosqueeze Toolbox (available for download:  
 172 <https://web.math.princeton.edu/~ebrevdo/synsq/>) which efficiently implements the SST  
 173 algorithm and offers a  $\log_2$  frequency resolution. They further tested the robustness  
 174 properties of SST and found that it precisely estimated key signal components, and that it  
 175 was stable against errors and noise (Thakur et al., 2013). The SST combines advantages of  
 176 the wavelet transform in regards to frequency resolution with the frequency reallocation  
 177 method (Auger and Flandrin, 1995) in order to reduce spectral smearing when mapping out  
 178 the frequency-time content of a complex signal. This presents a significant advantage when  
 179 identifying multiple frequency components over traditional methods such as the Fourier, or  
 180 more recently the Wavelet transform.

181

## Identification of continuous time periods featuring multiple distinct frequency components that are buried in a signal

Methodology steps	Comment
1. Measure parameter	For example drip discharge rate [ $M^3/T$ ], temperature [ $^{\circ}C$ ], barometric pressure [kPa]
2. Use the MATLAB Synchrosqueeze Toolbox (Thakur et al., 2013) to calculate the frequency domain response $\mathcal{F}_{f,t}$ $f$ is frequency (in $\log_2$ resolution) [ $1/T$ ] <ul style="list-style-type: none"> <li><math>t</math> is discrete time (sampling resolution) [T]</li> </ul>	The output is a 2D matrix containing the complex frequency domain response with elements corresponding to discrete frequency values (as rows) and time values (as columns)
3. Calculate signal amplitudes $A_{f,t} =  \mathcal{F}_{f,t}  = \sqrt{\Im(\mathcal{F}_{f,t})^2 + \Re(\mathcal{F}_{f,t})^2}$	Standard procedure to calculate the amplitude of a signal component (length of complex frequency domain vector)
4. Normalise signal amplitudes $a_{f,t} = \frac{A_{f_{min}<f<f_{max},t}}{\max(A_{f_{min}<f<f_{max},t})}$ $f_{min} = 0.48 \text{ and } f_{max} = 4.1$	The base for this normalisation allows focus on a desired frequency range. This is especially useful to identify continuous periods of weaker frequency components in the presence of other, stronger components or chaos
5. Visualise normalised amplitudes in pseudo-colour plot	Colour scale can be customised
6. Identify continuous time periods with multiple distinct frequency components based on the visual observation of continuous relative amplitudes in the desired frequency axis	While this step is conducted manually, it could be automated using criteria for the strength and continuity of any stable frequency component amplitudes of interest

182

183 **Figure 2:** Overview of the methodology applied to identify continuous time periods of  
 184 multiple distinct frequency components buried in a measured time series.

185 The drip discharge rate time series, barometric pressure and air temperature (potential  
 186 weather related drivers of drip discharge oscillations) were directly used as an input for the  
 187 MATLAB SST Toolbox. The calculated output is a complex frequency domain response, as is

188 common for signal component decomposition, but in matrix form  $\mathcal{F}_{f,t}$  mapped over  
189 frequency (rows) and time (columns). Amplitudes were calculated as the length of the  
190 complex frequency response vector  $A_{f,t} = |\mathcal{F}_{f,t}|$  and then normalised to obtain relative  
191 amplitudes  $a_{t,f}$ , using the maximum amplitude value occurring within the desired  
192 frequency range  $0.48 < f < 4.1$  and within the timespan of interest (e.g., plot). The  
193 relative amplitude of all parameters was visualised using pseudo-colour plots showing the  
194 spectral content of the signal. These plots allowed visual identification of key frequency  
195 components that could easily be distinguished from chaos, i.e. lack of regular oscillations  
196 identified as signals with varying amplitude and frequency over time. Stronger periodic  
197 components would yield a larger amplitude on the respective frequency scale and therefore  
198 also a colour that was closer to 1 in each of the SST plots (refer to the individual colour  
199 legends for values).

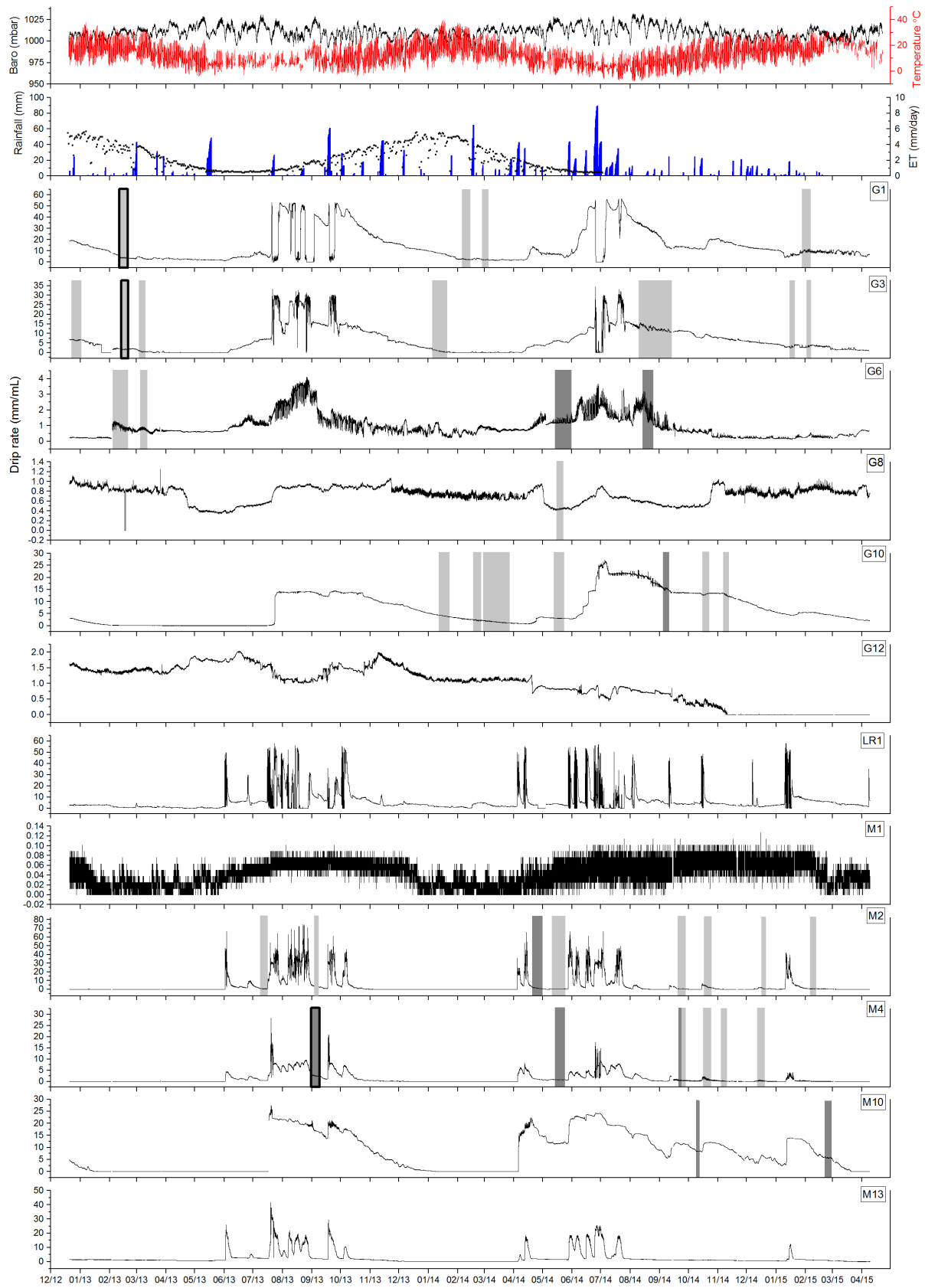
200 A periodic drip discharge rate could be defined as consisting of continuous periods of a)  
201 stable 1 cycle per day (cpd) frequency, b) stable 1 cpd and 2 cpd frequency, c) chaos  
202 (components with randomly varying frequency and amplitude). We used a) and b) as  
203 spectral “fingerprints” to identify and mark periods of continuous occurrence of daily and  
204 sub-daily oscillations in the drip discharge rate dataset. While identification of periodic  
205 signal components through visual inspection was subjective, it is based on a set of objective  
206 indicators such as normalised amplitude values and defined criteria. This methodology is  
207 summarised as a sketch in Figure 2 and could be applied to any type of time series in order  
208 to map the signal frequency content and identify periods with multiple distinct frequencies  
209 of interest.

210

### 211 **3. Results**

#### 212 **3.1 Drip discharge rate time series**

213 The drip discharge time series are presented in Fig. 32. The drip discharge sites are spatially  
214 clustered in three groups within the cave (Fig. 1 and Table 1). Sites with the G prefix are  
215 located near the main entrance of the cave on the western side. The location is highly  
216 decorated with speleothems. M sites are located in the middle section of the cave in a large  
217 chamber with a high ceiling populated by soda straw formations. Location LR1 is situated  
218 near the cave exit at the top of a flow stone.



219

220

221 Figure 32 Drip discharge rate time series for all drip sites in Glory Hole Cave with periods  
222 where daily fluctuations occur highlighted in light grey (1 cpd) and dark grey (1 cpd and 2  
223 cpd). The time periods examined in more detail in Fig. 43, 54 and 65 are indicated by bolder  
224 outline. Daily evapotranspiration (19/12/2012- 03/07/2014), rainfall, barometric, air  
225 temperature and are also shown.

226 The drip discharge rate at G1 and G3 varies seasonally, with higher drip rates in winter, total  
227 flow volume of 133.37 L and 109.52 L, respectively, - than summer (64.56 L and 14.1 L,  
228 respectively). Drip rate increases in response to rainfall events during the wet season and  
229 gradually decreases through the drier part of the year. Drip rate is lowest during April and  
230 May and highest during June and July. Similarly, G6 exhibits seasonal variation with a higher  
231 volume of discharge during the winter than summer. The drip rate at G10 increases sharply  
232 from 0.14 ml min<sup>-1</sup> on 21/07/2013 to 13.75 ml min<sup>-1</sup> on 29/07/2013, this drip rate is  
233 consistently sustained for 3 months indicated by the flat topped hydrograph (Fig. 32). From  
234 July 2013 onwards, the drip rate gradually decreases until June 2014 where it increases  
235 sharply again by an order of magnitude from 2.03 ml min<sup>-1</sup> on 3/06/2014 to 24.96 ml min<sup>-1</sup>  
236 on 4/07/2014. In May 2014, the drip rate again rapidly increases at G10 from 0.142 ml min<sup>-1</sup>  
237 to 21.59 ml min<sup>-1</sup> on 18/04/2014 and then proceeds to gradually decline until April 2015  
238 where it reaches baseline conditions. M10 exhibits similar behaviour with a low baseline  
239 drip rate which increases sharply during July 2013 and is sustained for ~3 months, however,  
240 the elevated drip rate decreases more rapidly than G10, returning to baseline conditions in  
241 January 2014. M1 has a very low drip rate ranging from 0- 0.13 ml min<sup>-1</sup> and is seasonally  
242 variable with higher drip rates during the winter. LR1, M2, M4 and M13 are very responsive  
243 to infiltration events and are characterised by a 'flashy' flow type, evidenced by the  
244 frequent spikes in drip rate. G12 has a low discharge rate which gradually decreases over  
245 the monitoring period until the site dries up completely in November 2014. There are small  
246 variations in drip rate that are not associated with rainfall events or seasonal drying. G8 is  
247 the only site which has a lower total flow volume during the winter (2013= 5.92 L; 2014= 5.7  
248 L) than summer (2014= 6.39 L; 2015= 6.84 L).

249

### 250 3.2 Characterisation of oscillations in the drip discharge rate

251 Daily fluctuations in drip discharge rate were identified in eight out of twelve sites using SST.  
252 There was no connection between the sites that did not exhibit the fluctuations with  
253 respect to spatial location, flow volume or flow regime type. The temporal and spatial  
254 pattern of daily oscillations are shown by the grey shaded areas in Fig. 32. The length of  
255 time the signal is present varied temporally for each drip site. For example, there was a  
256 strong 1 cpd signal in the drip water at G1 for 10 days in February 2013 whereas in January  
257 2014 1 cpd fluctuations only lasted 5 days (Fig. 4). The timing of when the signal occurs on  
258 an annual scale varied within and between drip sites. For example, a 1 cpd signal only  
259 occurred during the first 3 months of the year for G1, whereas a 1 cpd signal occurred

260 sporadically at G3 throughout the calendar year (December 2012, February and March  
261 2013, January 2014, September 2014, January 2015).

262 ~~The daily timing of minimum and maximum drip rates varied within and between individual  
263 drip sites. At G3 the 1 cpd minimum and maximum drip rate generally appeared between  
264 12-9 am and 3pm-12am, respectively. The minimum drip rate lagged 11-20 hours behind  
265 the timing of maximum evapotranspiration, which Burgess et al (2001) estimated to be 1  
266 pm. Daily oscillations were only observed once at G8 between 14-21/05/2014 with  
267 minimum drip rate appearing 3-9 am and maximum drip rate appearing between 12-9 pm.  
268 G6 exhibited a similar pattern with the exception of May and August 2014 where an  
269 additional 2 cpd signal was observed with the second peak following 3-6 hours later. Similar  
270 patterns of minimum drip rate lagging 11-20 hours behind the maximum daily  
271 evapotranspiration were exhibited at G10 (with weak 2 cpd between 5-16/10/2013) and M2  
272 (with weak 2 cpd between 20-28/04/2014). Both 1 cpd and 2 cpd signals were observed at  
273 M10 for all the periods of drip rate oscillation with the larger peak occurring in the  
274 afternoon between 3-6 pm and the smaller peak between 12-3 am, minimum drip rate  
275 appeared consistently between 6-9 am. In contrast, minimum drip rate at G1 was observed  
276 between 12-9 pm and maximum drip rate between 6-9 am indicating a lag time of  $\leq 9$  hours  
277 behind peak evapotranspiration. M4 was unique in that minimum drip rate are recorded  
278 between 6-9 am until October 2014 when it switches to 12-9 pm.~~

279 The daily timing of minimum and maximum drip rate varied within and between individual  
280 drip sites. At G1 the 1 cpd minimum and maximum drip rate generally appeared between  
281 12-9 am and 3pm-12am, respectively. Daily oscillations were only observed once at G8  
282 between 14-21/05/2014 with minimum drip rate appearing 9pm and maximum drip rate  
283 appearing around 12 pm. Both 1 cpd and 2 cpd signals were observed at M10 for all the  
284 periods of drip rate oscillation with the larger peak occurring in the afternoon between 12-6  
285 pm and the smaller peak between 12-6 am, minimum drip rate appeared consistently  
286 between 6-9 am. Time lag between drip rate and air temperature was quantified by  
287 performing a cross correlation analysis with a shift interval of 15 mins up to  $\pm 24$  hours  
288 (Table 2). The lag time was identified as the point of maximum negative correlation between  
289 the two variables with the exclusion of sites with missing data. At most sites the lag time  
290 between maximum air temperature and minimum drip rate varied greatly over the  
291 monitoring period. For example, at M4 initially the lag time was 24 hours in September  
292 2013, decreasing to 9 hours in May 2014 and eventually levelling off at around 16 hours  
293 from September to December 2014. In contrast, G1 had a similar lag time over all 4 periods  
294 of drip rate fluctuation ranging from 11.25- 12.75 hours. G6 was unique in that the  
295 minimum drip rate occurred before the maximum air temperature in February and March  
296 2013, January 2014 and 2015. Analysis of variance indicated that drip site and season did  
297 not explain a significant amount of variance in lag time.

298



299 Table 2 shows the time lag calculated using cross correlation analysis between air  
 300 temperature and daily drip rate for each period of drip rate oscillation.

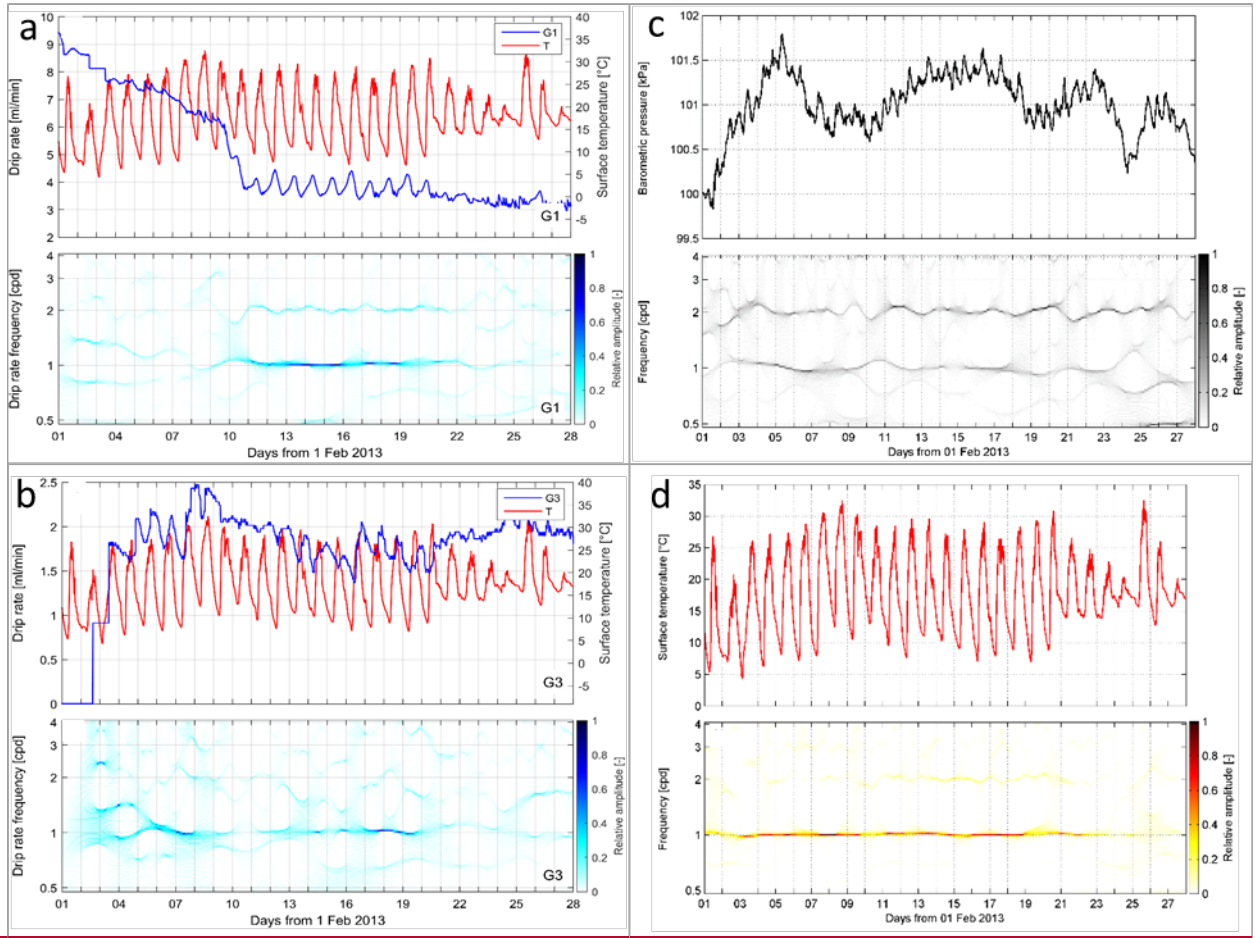
Site	Drip rate oscillation		Time lag (hours)	R <sup>2</sup>
	Start	End		
G1	11/02/2013	21/02/2013	-11.5	-0.82
	4/02/2014	14/02/2014	-12.75	-0.55
	27/02/2014	10/03/2014	-11.25	-0.37
	27/01/2015	5/02/2015	-11.5	-0.69
G3	23/12/2012	2/01/2013	-23.25	-0.46
	12/02/2013	20/02/2013	+2	-0.56
	4/03/2013	10/03/2013	+1	-0.44
	6/01/2014	20/01/2014	+7	-0.62
	20/09/2014	29/09/2014	-4	-0.38
	16/01/2015	20/01/2015	+0.25	-0.59
	3/02/2015	6/02/2015	+1	-0.74
G6	3/02/2013	19/02/2013	-4	-0.19
	5/03/2013	12/03/2013	-3.25	-0.51
	13/05/2014	29/05/2014	-21	-0.50
	14/08/2014	24/08/2014	-7	-0.50
G8	14/05/2014	21/05/2014	-9.5	-0.55
G10	5/10/2013	16/10/2013	-24	-0.40
	5/01/2014	22/01/2014	-0.5	-0.32
	18/02/2014	24/02/2014	-3	-0.46
	4/03/2014	23/03/2014	-2.75	-0.47
	13/05/2014	23/05/2014	-15	-0.37
	16/10/2014	22/10/2014	-23	-0.49
	8/11/2014	12/11/2014	-1.5	-0.59
	5/02/2015	25/02/2015	-0.25	-0.33
M2	3/09/2013	7/09/2013	-15.25	-0.76
	20/04/2014	28/04/2014	-1	-0.40
	13/05/2014	21/05/2014	-17.75	-0.60
	20/09/2014	28/09/2014	-23.75	-0.40
	18/10/2014	25/10/2014	-2	-0.31
	5/02/2015	10/02/2015	-20.75	-0.51
M4	2/09/2013	8/09/2013	-24	-0.46
	14/05/2014	23/05/2014	-9	-0.38
	21/09/2014	28/09/2014	-16.25	-0.59
	16/10/2014	24/10/2014	-16.25	-0.65
	4/11/2014	13/11/2014	-16.5	-0.62
	12/12/2014	22/12/2014	-16.5	-0.32
M10	23/12/2012	26/12/2012	-24	-0.32
	9/10/2014	12/10/2014	-4.75	-0.46

301

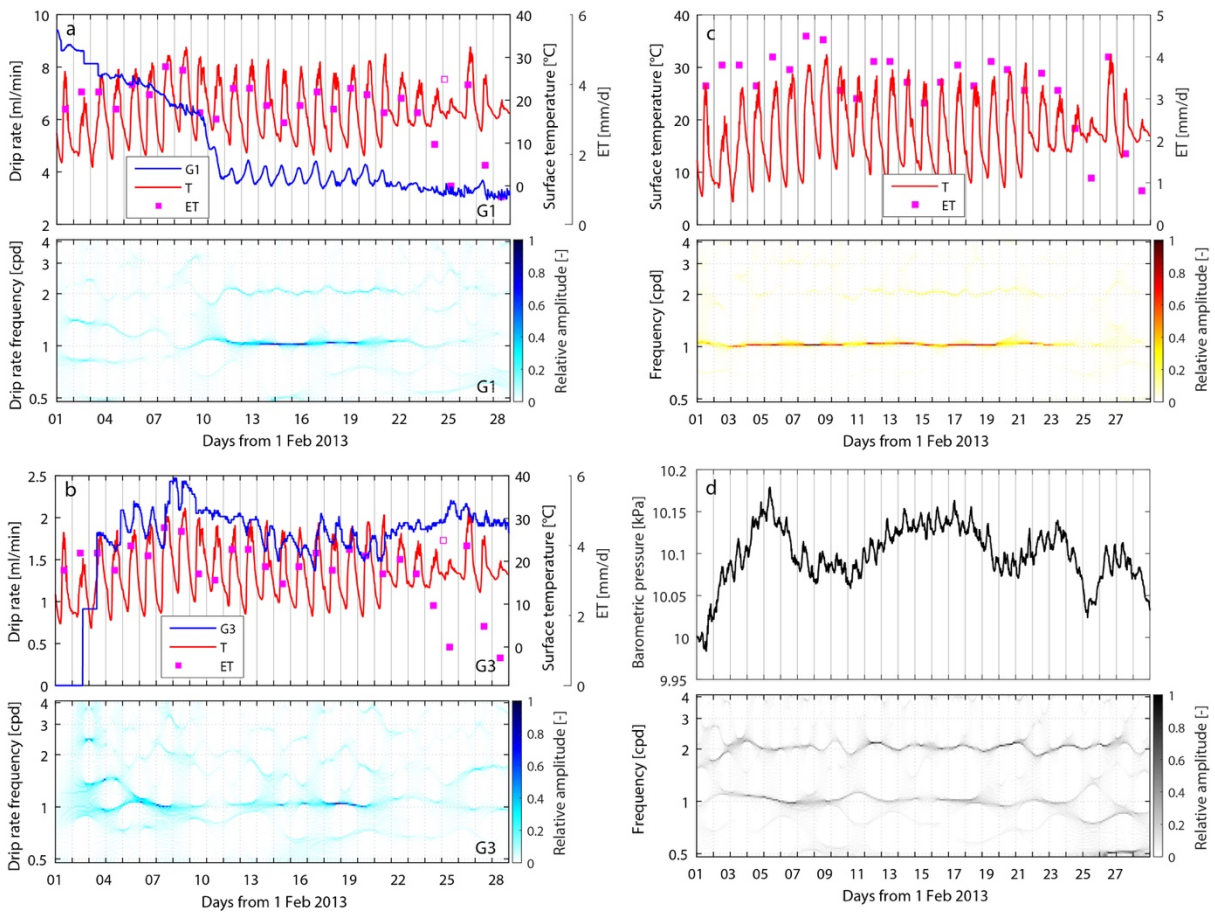
302

303 1 cpd and 2 cpd signals can occur concurrently, for example, at M4 between 1-9/9/2013  
304 (Fig. 54). This trend, where the 2 cpd is weaker than the 1 cpd is consistent across all sites  
305 where the two signals coincide. The 2 cpd signal can be visually determined in the raw drip  
306 rate data by a second smaller peak (Fig. 54). Examples of characteristic SST plots alongside  
307 the corresponding raw drip rate and surface temperature data will be discussed in greater  
308 detail below. All SST analyses have been plotted in the SI.

309



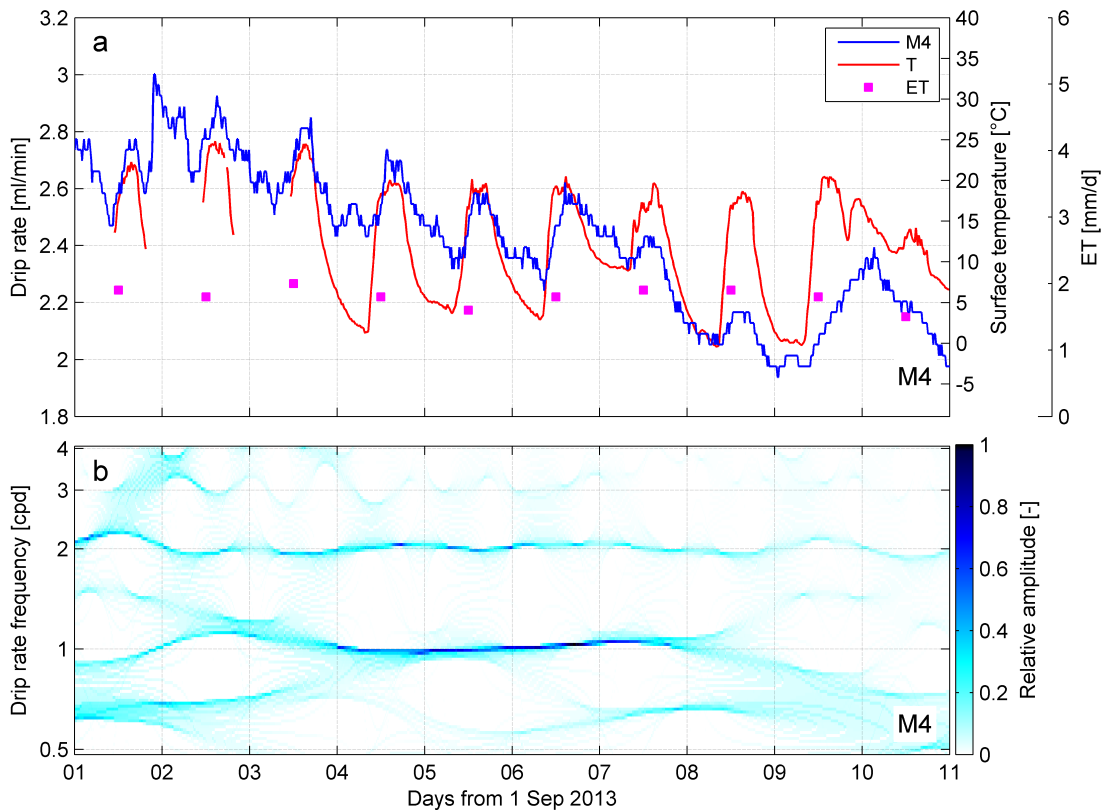
310



311

312 Figure 43 shows the raw drip rate, evapotranspiration and surface temperature data with  
 313 the corresponding drip rate synchrosqueezing plot for time periods where a 1 cpd signal is  
 314 present for sites a) G1 and b) G3 c) surface air temperature (T) and potential  
 315 evapotranspiration (ET) and d) barometric pressure for period February 2013.

316



318

319 Figure 54 shows the raw drip discharge data, evapotranspiration, surface temperature and  
 320 synchrosqueeze transform (SST) plot of the drip discharge for site M4 from 1-11/09/2013.

321 SST identified a 1 cpd oscillation in drip rate between 08/02/2013 and 21/02/2013 at G1 and  
 322 G3 (Fig. 43a, b). At G1 (Fig. 43a), the signal was initially chaotic, but from 08/02/13-  
 323 21/02/13 the drip rate oscillates sharply at 1 cpd. The maximum drip rate ranging from 4.03-  
 324 3.75 ml min<sup>-1</sup> occurred between 9:18 and 10:27 and the minimum drip rate ranging from  
 325 3.34 -3.75 ml min<sup>-1</sup> occurred between 18:39 and 21:27. The signal was chaotic from  
 326 21/02/2013.

327 The drip rate at G3 (Fig. 43b) oscillated at 1cpd for 8 days from 12/02/13-20/02/13. In  
 328 contrast to G1, the maximum drip rate appeared in the evening and the minimum drip rate  
 329 occurred in the morning. The maximum drip rate ranging from 1.63 -2.01 ml min<sup>-1</sup> occurred  
 330 between 20:21 and 00:40 and the minimum drip rate ranging from 0.36-0.48 ml min<sup>-1</sup>  
 331 occurred between 9:03 and 11:36 with the exception of 15/02/13 and 18/02/13 where it  
 332 appeared at 14:06 and 12:57, respectively. Similarly to G1, the 1 cpd trend  
 333 descended into chaos from 20/02/13 onwards. The maximum drip rate occurs between  
 334 14:23 and 22:45 and ranged from 0.53 to 1.14 ml min<sup>-1</sup>. The minimum drip rate occurred  
 335 between 01:18 and 11:32 and ranged from 0.228 to 0.95 ml min<sup>-1</sup>.

336

337 From 01-27/02/13, daily barometric pressure peaked between 8:30-9:00 with a magnitude  
338 of ~~~1-5 mbar~~0.1-0.5 kPa with a smaller second peak between 20:00-22:00 with a magnitude  
339 of ~~1-3~~0.1-0.3 mbar-kPa (Fig. 43c). There were larger changes in air pressure on a mesoscale  
340 with peaks in air pressure on 16/02/13, 22/02/13, 26/02/13 and minimum air pressure on  
341 19/02/13, 24/02/13 and 28/02/13. The air pressure changes in these cycles were as much as  
342 ~~15-20~~1.5-2 mbar-kPa. The drip rate at G1 and G3 did not appear to be affected by the daily  
343 or weekly changes in air pressure. For example, when air pressure decreased dramatically  
344 on 27/02/13 (Fig. 43c) there was no substantial change in drip rate at either G1 or G3.

345 Insolation drives daily cycles in surface air temperature with maximum temperatures  
346 recorded between 11:30-16:00 and minimum temperatures recorded between 4:00-8:00  
347 (Fig. 43d). The difference in daily minimum and maximum air temperature varied greatly.  
348 For example, between 12- 20/02/2013 the difference was 17.05-22.2 °C whereas between  
349 21- 27/02/2013, the temperature difference was as little as 4.5 °C. Evapotranspiration  
350 ranged from 0.8- 4.5 mm/day and was relatively high from 1-23/02/2013 with a slight  
351 downward trend which then decreased sharply on 23/02/2013 and 24/02/2013 to 2.3  
352 mm/day and 1.1 mm/day, respectively. Evapotranspiration had a strong correlation with  
353 maximum daily air temperature ( $R^2 = 0.59$ , p-value <0.05).

## 354 4. Discussion

### 355 4.1 Cave drip rate and karst architecture

356 The complexity of the Glory Hole Cave karst system is evident in the variety of drip regimes.  
357 For example, the drip rate at G1, G6 and G3 is seasonally driven with high discharge rates  
358 during the wettest period of the year. In contrast, drip discharge at G10 and M10 is likely  
359 driven by a storage component which discharges via a **less** permeable pathway which limits  
360 the store at a particular level during wet periods. The drip site is fed via the main water  
361 store rather than the overflow pathway itself (Baker et al., 2012; Bradley et al., 2010). Sites  
362 LR1, M4, M13 and M2 behave similarly in that they are all very responsive to rainfall events  
363 and have low base flows during periods of low rainfall. The response to rainfall events occur  
364 within 24 hours across these sites. Calculated flow volumes indicate the storage capacity of  
365 the stores feeding the discharge sites. For example, there was an infiltration event on  
366 01/06/2013 which caused a dramatic increase in drip rate for sites LR1, M2, M4 and M13.  
367 The flow volumes for each site from the start of the event to the point where the discharge  
368 returns to a constant rate are as follows LR1 (1.60 L), M4 (2.99 L), M13 (8.09 L) and M2  
369 (11.30 L). The length of the recession limb, **-calculated from the peak of the hydrograph until  
370 the drip rate returns to base rate**, is indicative of the speed at which the store drains. For  
371 example, the decay in drip rate is 12 days for site M2 compared to 4 days for M13. The time  
372 it takes for the store to drain is not dependent on flow volume, as M13 has a flow volume of  
373 more than 5 times that of site LR1 but they both have drainage periods of 5 days. The  
374 discrepancy in drainage time could indicate variation in flow pathway length between sites.  
375 G8 is the only site with a relatively lower total flow volume during winter than summer. M1  
376 has a low drip rate that shows a small seasonal fluctuation but does not visibly respond to  
377 individual events. This site is likely being fed by a store that is large enough to assimilate  
378 short term inputs from the surface without impacting drip rate. This type of store has been  
379 described ~~in~~**as a karst hydrological model component by in a number of studies (Arbel et**  
380 **al., 2010; Hartmann et al., 2014b; Markowska et al., 2015).**

381

### 382 4.2 Daily oscillations in drip rate

383 Constant frequency oscillations in drip discharge (1 cpd and 2 cpd) occur sporadically  
384 throughout the monitoring period December 2012- April 2015 at 8 out of 12 monitored drip  
385 sites. This phenomenon could be explained by a number of daily drivers including variations  
386 in pressure gradients between karst and cave due to cave ventilation effects, atmospheric  
387 and earth tides, or variations in hydraulic conductivity (due to changes in viscosity of water  
388 with daily temperature oscillations), and solar driven daily cycles of vegetative  
389 (phreatophytic) transpiration. These drivers are now considered in turn.

#### 390 4.2.1. Cave ventilation effects

391 Surface air pressure and cave air pressure were significantly correlated ( $\tau = 0.82$  significant at  
392 95%,  $n = 8939$ ) for the monitoring period 19/01/2015-08/09/2015. ~~A student's t test showed~~  
393 ~~that there was no significant difference between surface air pressure and cave air pressure~~  
394 ~~for the monitoring period 19/01/2015-08/09/2015 ( $p\text{-value} = 3.95 \cdot 10^{-6}$ ,  $n = 8939$ ).~~ This  
395 indicates that cave air exchange ("breathing" or ventilation) is very efficient and  
396 consequently that variations in air pressure between the cave and surface can be ruled out  
397 as driving the fluctuations in drip rate.

398

#### 399 4.2.2. Barometric loading

400 Atmospheric tides are caused by changes in air pressure due to the heating and cooling of  
401 air masses during the day and night. Correlations between atmospheric tides and drip rates  
402 can occur since increases (decreases) in atmospheric pressure at the ground surface are  
403 partitioned into stress increase (decrease) in the soil/rock mass and pore pressure increase  
404 (decrease) within the formation (Acworth et al., 2015). Drip rates could be affected if this  
405 changes the pressure gradient between the groundwater in karst stores and the cave  
406 (Tremaine and Froelich, 2013). Such a pressure imbalance is dependent on the  
407 hydromechanical properties and karst architecture as well as the degree of pneumatic  
408 connection between both the surface and the water table, and the surface and the cave at  
409 the location of the drip. Maximum and minimum atmospheric pressure occur at the same  
410 time each day (Fig. 4 ~~3d~~ **e**).

411 Atmospheric tides were eliminated as a process to explain the daily oscillation phenomenon  
412 for several reasons. Firstly, there was no relationship between drip discharge rate and the  
413 longer term barometric changes caused by synoptic weather patterns (Fig. 4 **e**). The  
414 mesoscale fluctuations in pressure caused by synoptic weather patterns are an order of  
415 magnitude higher than those caused by daily atmospheric tides. Since the drip rate did not  
416 respond to pressure changes of this size, they will not respond significantly to changes of a  
417 smaller magnitude at a higher frequency because higher frequency signals will be more  
418 highly damped and lagged. Secondly, the timing of the daily maximum and minimum drip  
419 rates in Glory Hole Cave varied within each drip site over time. For example, the peak  
420 discharge time for site G6 varied between 13:24 and 19:48 for the period 11/08/2013-  
421 25/08/2015. This finding contrasts with previous studies where drip rate is negatively  
422 correlated with barometric pressure and responds to daily pressure changes linearly  
423 (Tremaine and Froelich, 2013). However, this could indicate that the daily drip water  
424 variations in Glory Hole Cave are being driven by a non-linear process and this is discussed  
425 further below. Thirdly, the karst architecture of Glory Hole Cave is well-developed, has little  
426 to no primary porosity and is unconfined. Hence, it is unlikely to exhibit barometric  
427 responses such as seen in confined systems (Merritt, 2004), whereby pore pressure changes  
428 due to barometric loading are substantially lower than the change of cave air pressure.



429

#### 430 **4.2.3. Earth tides**

431 Earth tides are solid deformations of the Earth's surface caused by the gravitational pull of  
432 the moon and sun (Merritt, 2004). It has been previously shown that earth tides can cause  
433 regular oscillations in groundwater level if the aquifer is sufficiently confined (Acworth et al.,  
434 2015). However, at Glory Hole Cave this process can be ruled out due to the unconfined  
435 conditions, the fact that the compressibility of limestone is smaller than that of water, and  
436 because fluctuations in pressure caused by earth tides are so small.

437

#### 438 **4.2.4. Temperature driven viscosity influences on hydraulic conductivity**

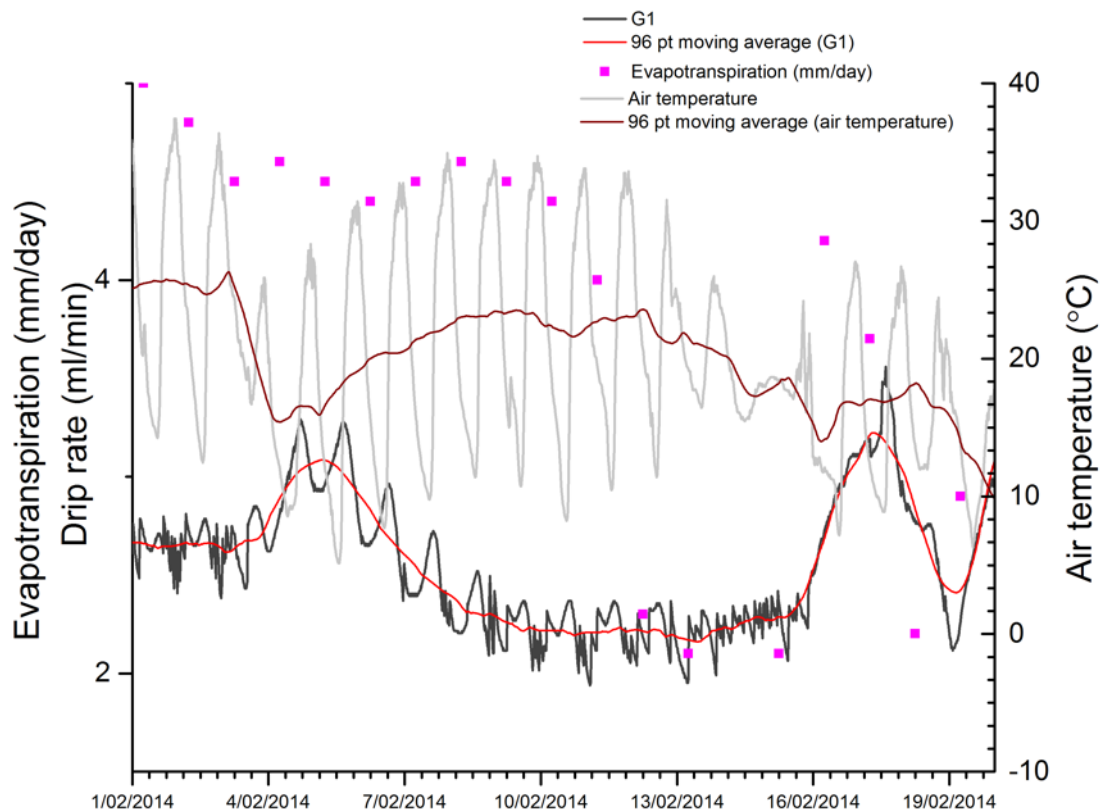
439 The study site has large surface temperature variations, particularly in summer where day  
440 time and night time temperatures can vary up to 31.1 °C. Consequently, the dynamic  
441 viscosity of water could range from 0.8- 1.79 x 10<sup>-3</sup> Pa s (based on a temperature range from  
442 30-0 °C, respectively). However, the conductive propagation in diel temperature variations  
443 are expected to be highly attenuated with depth (Rau et al., 2015) resulting in almost  
444 complete damping by 1 m bgl. Furthermore, the daily temperature range within the cave  
445 itself is just 0.08-1.53 °C, primarily due to air exchange moderated by conductive  
446 equilibrium with the cave walls. The variation of water viscosity (which is inversely  
447 proportional to hydraulic conductivity) is approximately 2 to 3 % per degree in the range  
448 10 to 30 °C. Considering that the amplitude of a 1 cpd drip rate fluctuation can be as much  
449 as 75 % of the maximum drip rate, the greatest anticipated change in hydraulic conductivity,  
450 and therefore the drip rate (proportional to the hydraulic conductivity by Darcy's law), on a  
451 daily cycle, is likely to be 2-3 orders of magnitude lower than the observed variation in drip  
452 rate on a daily basis. We therefore conclude that the daily fluctuations in drip rate are  
453 unlikely to be caused by variations in hydraulic conductivity due to changes in viscosity of  
454 water.

455

#### 456 **4.2.5. Solar driven daily cycles of vegetative (phreatophytic) evapotranspiration**

457 The timing of the daily drip rate signal appears to be associated with the difference in  
458 maximum and minimum surface temperature. In the examples examined in more depth in  
459 Fig. 43a-b, when the difference between the maximum and minimum temperature was high  
460 (17.05- 22 °C) and the evapotranspiration was relatively high (mean 3.6 mm/day) the 1cpd  
461 signal was **strongcontinuous**. Conversely, when the temperature difference was small (4.5-  
462 12.7 °C) and the **potential** evapotranspiration was relatively lower (mean 2.2 mm/day), the 1  
463 cpd signal dissolved into chaos.

464 During periods when there are 1 cpd oscillations in drip rate, there ~~wasis~~ was a relationship  
 465 between drip rate and surface temperature on a weekly timescale. ~~The bestFor~~ For example, in  
 466 Fig. 65 where  $\tau = -0.21$  (significant at 95%) for a 2-day average air temperature and drip rate  
 467 at G1 from 01-19/02/2014. ~~there is a negative relationship between the daily moving~~  
 468 ~~averages for surface air temperature and drip rate at G1 from 01-19/02/2014.~~ We have  
 469 demonstrated above that it cannot be air temperature driving the signal through either  
 470 atmospheric tides or water viscosity changes. However, the relationship between surface  
 471 temperature variability and 1 cpd drip rate oscillations could be explained if the association  
 472 with diurnal temperature variability is due to variations in solar radiation received at the  
 473 surface, as it is solar radiation which primarily drives photosynthesis and thus transpiration  
 474 in vegetation. This is confirmed by the strong positive relationship between daily solar  
 475 radiation and ~~potential~~ evapotranspiration ( $R^2 = 0.59$ , p-value  $< 0.05$ ).



476

477 Figure 6 shows the surface air temperature, evapotranspiration and drip discharge rate with  
 478 the corresponding daily moving average for site G1 01/02/2014-19/02/2014.

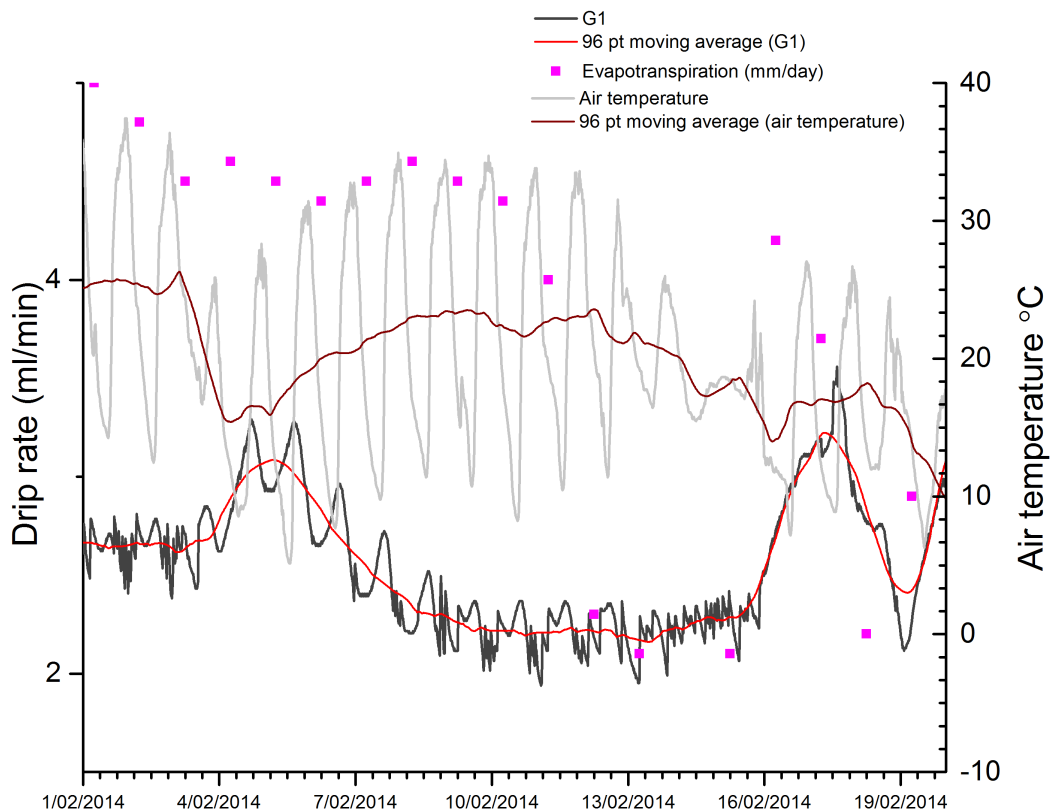
479

480 Daytime solar radiation receipt is highest in the absence of cloud cover, because there is no  
 481 barrier to incoming ~~long wave and~~ short wave radiation which leads to the heating of the  
 482 earth's surface and atmosphere, resulting in higher air temperature. Due to the lack of cloud

483 cover, night-time cooling occurs because of the ~~loss of~~ heat loss through outgoing long wave  
484 radiation, therefore periods of high daytime solar radiation are characterised by large air  
485 temperature amplitudes. In comparison, solar radiation received at the earth's surface is  
486 low in the presence of cloud cover because of the high albedo of clouds. In this case, there is  
487 a smaller temperature amplitude because clouds reduce the amount of incoming short  
488 wave ~~and longwave~~ radiation during the day, reducing daytime temperatures and reduce  
489 the amount of outgoing longwave radiation and effectively "insulating" the air at night  
490 leading to relatively warmer temperatures at night.

491 During periods of high solar radiation, plants photosynthesise more and therefore use more  
492 water. We hypothesise that firstly, tree water use was driving the intermittent daily  
493 oscillations in drip discharge demonstrated by the relationship between daily to weekly  
494 variations in surface air temperature and drip discharge and secondly, the sporadic nature  
495 of the oscillations was driven by complexities in the karst architecture. It has been widely  
496 accepted that tree water use causes fluctuations of the water table (Gribovszki et al 2010;  
497 Acworth et al 2015). However, this is the first study that shows tree water use affecting cave  
498 drip water.

499 The area above the cave and in the small uphill catchment is dominated by *E. pauciflora* and  
500 *E. stelullata* (Fig. 1). Eucalypt species have a bimodal root systems with shallow lateral roots  
501 and vertically descending roots which penetrate into the profile to depths of up to 18 m,  
502 with depth depending on soil characteristics and the degree to which the bedrock is  
503 fractured and ~~/~~conduits developed (Crombie, 1992; Farrington et al., 1996). Hence, these  
504 trees have the mechanism to abstract water from karst stores at depth which supports our  
505 theory that tree water use causes daily oscillations in cave drip rate.



506

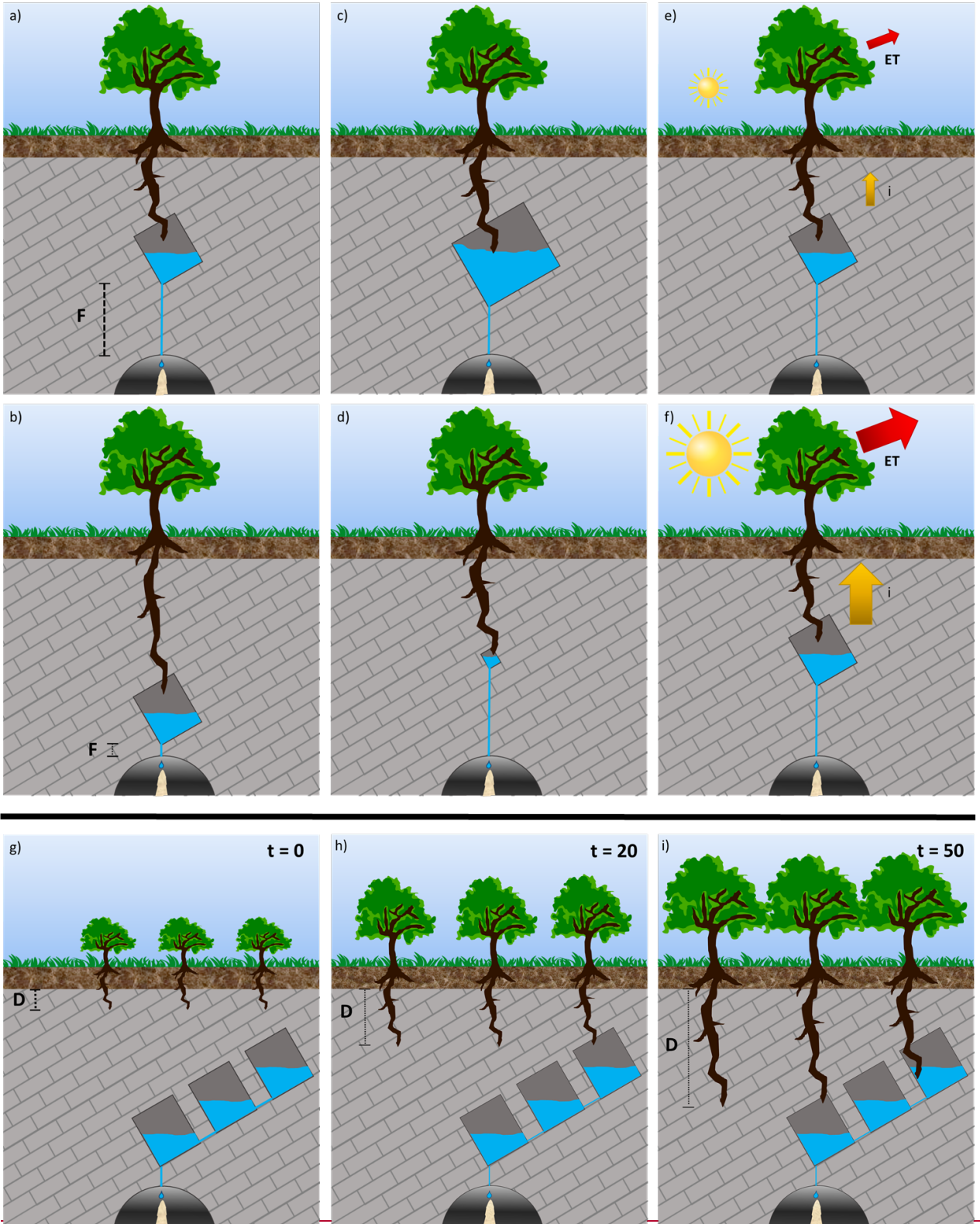
507 ~~Figure 5 shows the surface air temperature, evapotranspiration and drip discharge rate with~~  
 508 ~~the corresponding daily moving average for site G1 01/02/2014 19/02/2014.~~

509

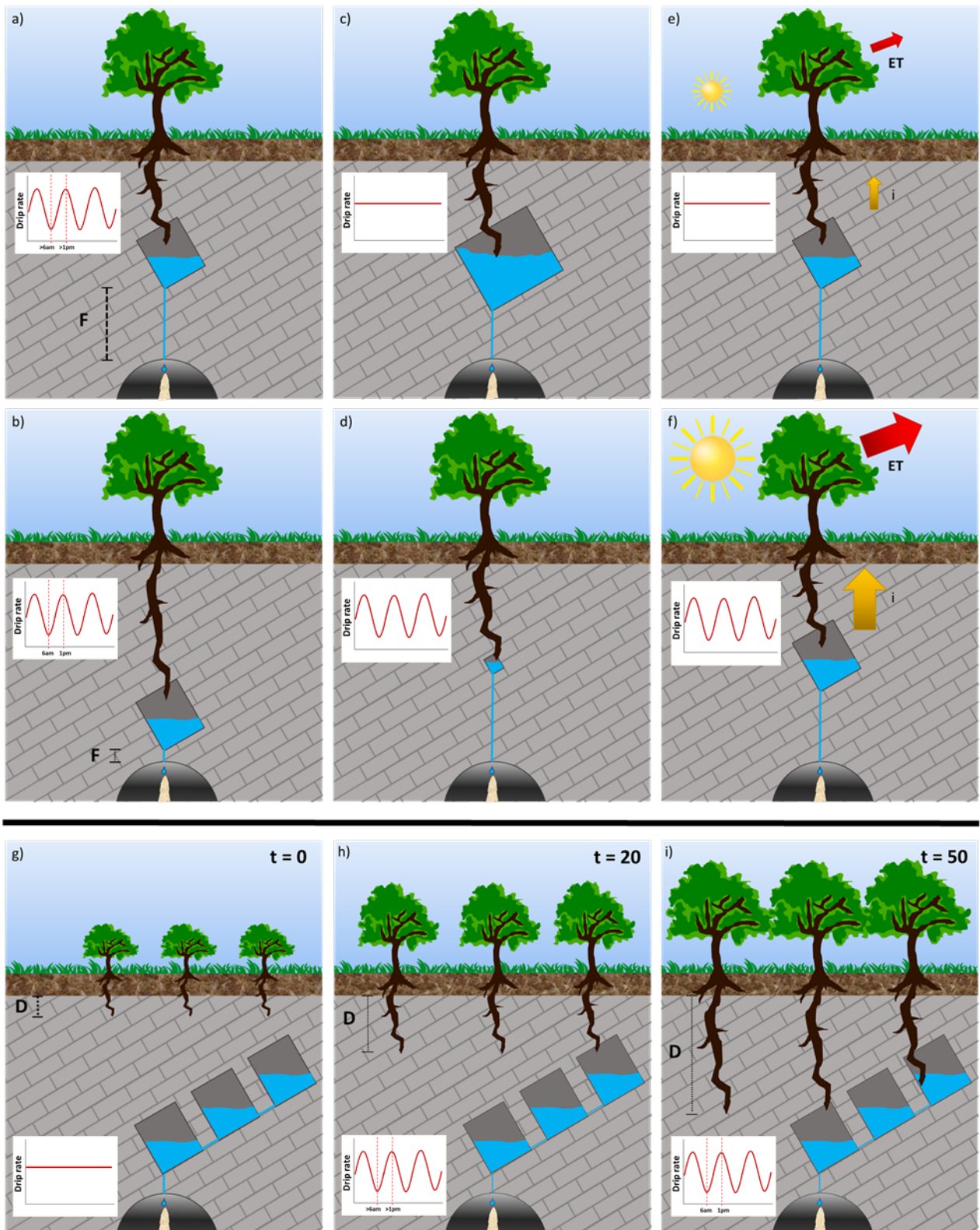
510 Tree water use from deep roots occurs when the upper layers are too dry and have a lower  
 511 water potential than the soil water at deeper levels (Dawson and Pate, 1996; Zapater et al.,  
 512 2011) ~~increases with the need for the tree to obtain water, and this will increase with~~  
 513 ~~increasing transpiration and solar radiation (O'Grady et al., 1999).~~ Maximum tree water use  
 514 by the roots is therefore expected in the afternoon during the period of maximum solar  
 515 radiation, possibly lagged due to the time taken to hydraulically lift the water. Conversely,  
 516 minimum tree water use is expected at the end of night around 6am. Burgess et al (2001)  
 517 measured sap flow in Eucalypt tap roots, finding ~~positive hydraulic lift~~ tap root sap flow  
 518 peaked around 1 pm and ~~a negative hydraulic lift~~ negative sap flow values indicated reverse  
 519 (acropetal) flow between 7pm- 7am. In consideration of this, drip water that comes from  
 520 fractures and stores which contain tree roots would be expected to have a minimum drip  
 521 discharge in the afternoon and maximum around sunrise. In reality, we observe more  
 522 complex daily drip oscillations, with peak drip rate occurring at different times of the day  
 523 and different times of the year. This is to be expected from a karstified system with flow  
 524 routed through a varied and complex fractured network. Different scenarios ~~for driving~~ daily  
 525 oscillations in a karst system will be discussed in detail below.

526 **4.2.5.1 Scenarios for solar driven daily cycles of phreatophytic evapotranspiration**

527



528  
529



530

531 Figure 76 shows a conceptual representation of tree water use from karst stores under  
 532 different circumstances. a) and b) show different karst store-drip site flow path lengths (F)  
 533 as the tree roots access karst stores at different depths; c) and d) show tree roots accessing  
 534 karst stores with different volumes; the influence of annual insolation on evapotranspiration  
 535 (ET) and hydraulic lift (i) during winter and summer is shown in e) and f) respectively. Finally,

536 the increase in rooting depth (L) and access to deeper karst stores over time in years (t) is  
537 explored in g-i.

538 The depth of a store could affect the timing of daily drip rate oscillations due to the delay in  
539 tree water transport. For example, consider the hypothetical, identical trees with roots  
540 intercepting identical karst stores or fractures at *different* depths in Fig. 76a and 76b. There  
541 is likely to be a greater lag in drip response in Fig. 76a than Fig. 76b because of the longer  
542 flow path-length (F) from the tree root to the cave drip site. Given that eucalypt tap roots  
543 can penetrate to depths ranging from 5-20 m with tap root length depending on the depth  
544 of accessible water (Carbon et al., 1980; Dawson and Pate, 1996) and the drip sites at Glory  
545 Hole Cave are located 30-50 m below the surface, we can speculate that the minimum flow  
546 path length between a taproot accessing the karst store and the drip site below could vary  
547 from 10-45 m. In reality, it is difficult to calculate exact flow path length because of the  
548 prevalence of lateral flow in heavily karstified systems. This has been demonstrated by  
549 Markowska et al (2016) in a study where water spiked with a tracer was used to irrigate the  
550 surface above a cave resulting in a response at discharge sites located 7 m laterally from the  
551 irrigation location. ~~At all drip discharge sites~~ Across all sites, lag time between maximum air  
552 temperature and minimum drip rate ranged from 0.25- 24 hours (Table 2) ~~the minimum drip~~  
553 ~~discharge rate is lagged by 12-18 hours from when we would expect the peak transpiration~~  
554 ~~to occur at 1pm. The exception is G1 where the minimum discharge rate occurs between~~  
555 ~~12-9 pm indicating a lag time of  $\leq 9$  hours.~~ We can hypothesise that ~~G1~~ those sites with a  
556 shorter lag time have a ~~has a~~ shorter path length from tree root accessed store to cave  
557 discharge site than the other drip sites. For example, the lag time for site G1 ranges from  
558 11.25- 12.75 hours whereas site G10 ranges from 0.5- 3 hours. This process could also  
559 explain ~~the unique case of M4 where the timing of minimum and maximum drip rate during~~  
560 ~~a 1 cpd oscillation switches in October 2014~~ the large variation in lag time within a particular  
561 site, for example at G6 the lag time was 21 hours in May 2014 and decreased to 7 hours in  
562 August 2014 (Table 2). ~~(Fig. 2).~~ We hypothesise that the change is due to a shortening of the  
563 path length from root accessed store to cave discharge site as the tree grows and increases  
564 its rooting depth, thus accessing a deeper water store.

565 The size of the karst store, or volume of water within the store, could determine whether  
566 the daily oscillation is observable or not. Consider the conceptual Fig. 76c and 76d, where  
567 identical trees have roots intercepting different karst stores at the *same* depth. We  
568 ~~hypothesise-propose~~ that a daily oscillation will only be observed when the tree water use is  
569 a significant part of the total water store so a daily oscillation is more likely to be observed  
570 in the smaller store (Fig. 76d) than a store with a larger volume (Fig. 76c). The influence of  
571 store volume on the presence of daily oscillations could also explain why the phenomenon is  
572 not observed at M1. In section 3.1 we discuss how the low, consistent drip rate at M1  
573 responds to seasonal drying but does not respond to individual rainfall events. We propose  
574 that this site is fed by a store large enough to assimilate individual rainfall events and the  
575 same line of reasoning could explain the lack of response to tree water use, the volume of



576 water extracted by tree roots is insignificant in relation to the large volume of water in the  
577 store. Conversely, we can hypothesise that G6 has a small store volume that is more  
578 sensitive to water uptake by tree roots, which is why we see the minimum drip rate  
579 occurring 0.25-7 hours before peak air temperature (Table 2). Furthermore, tThis scenario is  
580 supported by the fact that, generally, the daily oscillations are not exhibited during periods  
581 of high rainfall, and consequently high drip discharge, as the tree use signal is more likely to  
582 be a smaller fraction of the total water volume. Sites G1, G3 M2 and M4 have high seasonal  
583 discharge rates during June-September as indicated by the multiple hydrograph peaks for  
584 the corresponding sites in Fig. 32. There are no daily oscillations during these periods of  
585 peak discharge at any of these sites. Daily oscillations coincide with the receding limb of the  
586 peak at sites M4 (July and September 2013) and M4 (September 2013) as the drip rate  
587 decreases. ~~The influence of store volume on the presence of daily oscillations could also~~  
588 ~~explain why phenomenon is not observed at M1. In section 3.1 we discuss how the low,~~  
589 ~~consistent drip rate at M1 responds to seasonal drying but does not respond to individual~~  
590 ~~rainfall events. We propose that this site is fed by a store large enough to assimilate~~  
591 ~~individual rainfall events and the same line of reasoning could explain the lack of response~~  
592 ~~to tree water use, the volume of water extracted by tree roots is insignificant in relation to~~  
593 ~~the large volume of water in the store.~~The non-observance of daily oscillations during  
594 periods of high rainfall could also be attributed to the redistribution of water by the roots  
595 from the saturated soil to the unsaturated subsurface (Burgess et al., 2001).

596 Tree water use responds to annual variation in insolation. Consider Fig. 76e and Fig. 76f  
597 where one tree root intercepts the same karst store over the course of a year. During winter  
598 (Fig 76e), there is less insolation than the summer (Fig 76f) therefore the rate of  
599 evapotranspiration is lower. This means that in winter the hydraulic lift (i) is low or negative  
600 and daily oscillations in drip discharge could be dampened or absent. Our analysis reveals  
601 that only 2 out of 41 periods of 1 cpd oscillation occur during winter months June-August  
602 (G6 between 14-24/8/13 and M2 between 8-13/7/2013). However, our analysis also  
603 revealed that season did not explain a significant amount of variance in lag time, thus  
604 suggesting that more variables, such as karst architecture, are affecting the timing of drip  
605 rate oscillations.

606 In reality, there are multiple trees of different ages above the cave, further complicating the  
607 flow variability. Figure 76g-i presents a conceptual representation of tree tap root length  
608 increasing (L) as the tree grows and accesses deeper karst stores over 0-50 yr timescale (t).  
609 This response to annual insolation and the interaction of multiple trees of varying ages could  
610 explain why daily oscillations at an individual drip site occur one year and not the next, for  
611 example at M10 there is a 1 cpd in December 2012 however, this oscillation does not occur  
612 at the same time in 2013 or 2014. The mechanism in Fig. 76i could also explain why 2 cpd  
613 signals are also observed, whereby multiple tree roots are accessing interconnected water  
614 stores at different depths resulting in two separate cycles with differing lag times. The  
615 occurrence of 2 cpd signals in drip rate could also be related to signal processing where if

616 the signal is not strictly sinusoidal there may be harmonics in the spectrum. This finding and  
617 the interpretation is an area for further research.

#### 618 **4.6 Implications for karst architecture and climate proxy modelling research**

619 Karst architecture controls flow regimes and drip discharge rates of water ~~in~~filtrating into  
620 caves (e.g., Markowska et al., 2015). Flow rate influences speleothem climate proxies, such  
621 as the  $\delta^{18}\text{O}$  and concentration of solutes in drip water, through the dilution and mixing of  
622 percolation waters prior to reaching the cave. It is important to distinguish between the  
623 influence of karst architecture and climate-driven processes, such as drought, on discharge  
624 so that paleoclimate proxy records from associated speleothems can be appropriately  
625 constrained. This study has increased our understanding of karst architecture, information  
626 which can be utilised in proxy-system models or forward models, approaches that are  
627 increasingly used to understand cave drip rate variability and to model speleothem proxies  
628 such as  $\delta^{18}\text{O}$  (Bradley et al., 2010; Cuthbert et al., 2014a). Additionally, we propose that an  
629 important part of any protocol for inferring karst architecture is 1) the incorporation of cave  
630 drip rate monitoring with a minimum 15 min interval at multiple discharge sites for at least a  
631 year and 2) the systematic investigation of daily, weekly and monthly timescales using  
632 frequency analysis capable of showing frequency-time changes, such as the synchrosqueeze  
633 transform (Daubechies et al., 2011) to infer karst flow processes and their relative  
634 importance. **This study clearly demonstrates the potential for vegetation to impact karst  
635 water recharge making this research relevant to karst modelling and karst water resources  
636 assessment. Currently, there are no approaches that consider the impacts of vegetation on  
637 recharge dynamics in process-based karst models (Hartmann et al., 2014b, 2015) or in  
638 empirical recharge estimation approaches (Allocca et al., 2014; Andreo et al., 2006).**

639 This is the first volumetric observation of tree water use in cave drip water. This supports a  
640 growing number of studies examining the impact of trees on karst processes and  
641 paleoclimate proxies. For example, tree root respiration provides a source of  $\text{CO}_2$  for the  
642 dissolution of limestone that is additional to that from soil and vadose zone microbial  
643 respiration. Coleborn et al (2016) found that vegetation regeneration determined post-fire  
644 soil  $\text{CO}_2$  in a study investigating post-fire impacts on karst processes. Direct observations of  
645 tree water use within the karst unsaturated zone implies the presence of root respiration, a  
646 process which in turn affects drip water and speleothem  $^{14}\text{C}$  and  $\delta^{13}\text{C}$  composition (Fairchild  
647 and Baker, 2012; Meyer et al., 2014; Noronha et al., 2015). Trees have been demonstrated  
648 to have long-term effects on cave drip-water solute concentrations. Treble et al. (2015,  
649 submitted) demonstrate long-term trends in drip water calcium and trace element  
650 concentration, which they attribute to increasing solute concentration due to forest  
651 regrowth and increased post-fire tree water use. Baldini et al (2005) infer an effect on  
652 speleothem  $\delta^{18}\text{O}$  due to secondary forest regrowth after mining and Wong and Banner  
653 (2010) found clearing surface vegetation changed drip water Mg/Ca and Sr/Ca. The findings

654 and suggested protocol in this study will inform the selection of speleothem specimens for  
655 further research into the impact of tree water use on speleothem paleoclimate proxies.

## 656 **5. Conclusions**

657

658 We demonstrated a novel method of analysing recurring patterns in cave water drip rate  
659 using the synchrosqueezing transform (SST). Our analysis revealed daily and sub-daily  
660 oscillations with variable temporal and spatial signatures. We tested competing hypotheses  
661 for causes of daily oscillations using drip rate, barometric and temperature data. The only  
662 hypothesis which all the data and hydrogeologic theory were consistent, was that daily  
663 fluctuations in drip rate were driven by tree water use. We proposed that the complexity of  
664 flow pathways in the karst system accounted for the spatial and temporal variation in the  
665 daily fluctuations of drip rate. This was explored in detail using conceptual models. The  
666 results have wider implications for karst research including providing a new protocol for  
667 inferring karst architecture ~~and~~, informing selection of speleothem specimens for tree  
668 water use paleoclimate studies **and highlighting the importance of vegetation dynamics on**  
669 **karst recharge.**

670

## 671 **Author contribution**

672 KC, MOC, GCR and AB wrote the manuscript, discussed the results and implications and  
673 commented on the manuscript at all stages. KC, AB and ON collected data. GCR performed  
674 the SST analysis and generated the SST figures. GCR and ON created the location map. KC  
675 generated other graphs and conceptual figures.

## 676 **Acknowledgements**

677 We acknowledge that Katie Coleborn was supported the Australian Research Council  
678 (LP130100177). Mark Cuthbert was supported by Marie Curie Research Fellowship funding  
679 from the European Community's Seventh Framework Programme [FP7/2007-2013] under  
680 grant agreement n.299091. We would also like to thank Stuart Hankin for allowing us access  
681 to the weather station data and the National Parks and Wildlife Service staff at Yarrangobilly  
682 Caves. Solar exposure data derived from satellite imagery processed by the Bureau of  
683 Meteorology from the Geostationary Meteorological Satellite and MTSAT series operated by  
684 Japan Meteorological Agency and from GOES-9 operated by the National Oceanographic &  
685 Atmospheric Administration (NOAA) for the Japan Meteorological Agency. **We would also**  
686 **like to acknowledge the use of equipment funded by the Australian Government National**  
687 **Collaborative Research Infrastructure Strategy (NCRIS).**

## 688 **References**

689 Acworth, R. I., Rau, G. C., McCallum, A. M., Andersen, M. S. and Cuthbert, M. O.:

690 Understanding connected surface-water/groundwater systems using Fourier analysis of  
691 daily and sub-daily head fluctuations, *Hydrogeol. J.*, 23(1), 143–159, doi:10.1007/s10040-  
692 014-1182-5, 2015.

693 Adamson, L. and Loudon, A.: Wagga Geological Sheet, SI/55-15, 1st edition, 1:250000, 1966.

694 Allocca, V., Manna, F. and De Vita, P.: Estimating annual groundwater recharge coefficient  
695 for karst aquifers of the southern Apennines (Italy), *Hydrol. Earth Syst. Sci.*, 18(2), 803–817,  
696 doi:10.5194/hess-18-803-2014, 2014.

697 Andreo, B., Vias, J., Duran, J. J. and Jimenez, P.: Methodology for groundwater recharge  
698 assessment in carbonate aquifers: application to pilot sites in southern Spain, *Hydrogeol. J.*,  
699 16, 911–925, 2006.

700 Arbel, Y., Greenbaum, N., Lange, J. and Inbar, M.: Infiltration processes and flow rates in  
701 developed karst vadose zone using tracers in cave drips, *Earth Surf. Process. Landforms*,  
702 35(14), 1682–1693, doi:10.1002/esp.2010, 2010.

703 Auger, F. and Flandrin, P.: Improving the readability of time-frequency and time-scale  
704 representations by the reassignment method, *IEEE Trans. Signal Process.*, 43(5), 1068–1089,  
705 doi:10.1109/78.382394, 1995.

706 Baker, a., Bradley, C., Phipps, S. J., Fischer, M., Fairchild, I. J., Fuller, L., Spötl, C. and Azcurra,  
707 C.: Millennial-length forward models and pseudoproxies of stalagmite  $\delta^{18}\text{O}$ : an example  
708 from NW Scotland, *Clim. Past*, 8(4), 1153–1167, doi:10.5194/cp-8-1153-2012, 2012.

709 Baker, A. and Brunsdon, C.: Non-linearities in drip water hydrology: an example from Stump  
710 Cross Caverns, Yorkshire, *J. Hydrol.*, 277(3-4), 151–163, doi:10.1016/S0022-1694(03)00063-  
711 5, 2003.

712 Baldini, J. U. L., McDermott, F., Baker, a, Baldini, L. M., Matthey, D. P. and Railsback, L. B.:  
713 Biomass effects on stalagmite growth and isotope ratios: A 20th century analogue from  
714 Wiltshire, England, *Earth Planet. Sci. Lett.*, 240(2), 486–494, doi:10.1016/j.epsl.2005.09.022,  
715 2005.

716 Baldini, J. U. L., McDermott, F., Baldini, L. M., Ottley, C. J., Linge, K. L., Clipson, N. and Jarvis,  
717 K. E.: Identifying short-term and seasonal trends in cave drip water trace element  
718 concentrations based on a daily-scale automatically collected drip water dataset, *Chem.*  
719 *Geol.*, 330-331, 1–16, doi:10.1016/j.chemgeo.2012.08.009, 2012.

720 Bradley, C., Baker, A., Jex, C. N. and Leng, M. J.: Hydrological uncertainties in the modelling  
721 of cave drip-water  $\delta^{18}\text{O}$  and the implications for stalagmite palaeoclimate reconstructions,  
722 *Quat. Sci. Rev.*, 29(17-18), 2201–2214, doi:10.1016/j.quascirev.2010.05.017, 2010.

723 Burgess, S. S. O., Adams, M. a., Turner, N. C., White, D. a. and Ong, C. K.: Tree roots:  
724 Conduits for deep recharge of soil water, *Oecologia*, 126(2), 158–165,  
725 doi:10.1007/s004420000501, 2001.

726 Carbon, B. A., Bartle, G. A., Murray, A. M. and Macpherson, D. K.: The distribution of root  
727 length, and the limits to flow of soil water to roots in a dry sclerophyll forest, *For. Sci.*, 26(4),  
728 656–664, 1980.

- 729 Collister, C. and Matthey, D.: Controls on water drop volume at speleothem drip sites: An  
730 experimental study, *J. Hydrol.*, 358, 259–267, doi:10.1016/j.jhydrol.2008.06.008, 2008.
- 731 Crombie, D. S.: Root depth, leaf area and daytime water relations of Jarrah (*Eucalyptus*  
732 *marginata*) forest overstorey and understorey during summer drought, *Aust. J. Bot.*,  
733 40(1988), 113–22, doi:10.1071/BT9920113, 1992.
- 734 Cuthbert, M., Baker, A., Jex, C., Graham, P., Treble, P., Andersen, M. and Acworth, I.: Drip  
735 water isotopes in semi-arid karst: Implications for speleothem paleoclimatology, *Earth*  
736 *Planet. Sci. Lett.*, 395, 194–204, doi:10.1016/j.epsl.2014.03.034, 2014a.
- 737 Cuthbert, M. O., Rau, G. C., Andersen, M. S., Roshan, H., Rutledge, H., Marjo, C. E.,  
738 Markowska, M., Jex, C. N., Graham, P. W., Mariethoz, G., Acworth, R. I. and Baker, A.:  
739 Evaporative cooling of speleothem drip water., *Sci. Rep.*, 4, 5162, doi:10.1038/srep05162,  
740 2014b.
- 741 Daubechies, I., Lu, J. and Wu, H. T.: Synchrosqueezed wavelet transforms: An empirical  
742 mode decomposition-like tool, *Appl. Comput. Harmon. Anal.*, 30(2), 243–261,  
743 doi:10.1016/j.acha.2010.08.002, 2011.
- 744 Dawson, T. E. and Pate, J. S.: Seasonal water uptake and movement in root systems of  
745 Australian phraeatophytic plants of dimorphic root morphology: a stable isotope  
746 investigation, *Oecologia*, 107(1), 13–20, doi:10.1007/BF00582230, 1996.
- 747 Fairchild, I. J. and Baker, A.: *Speleothem Science: From Process to Past Environments*, 1st  
748 ed., Wiley-Blackwell., 2012.
- 749 Fairchild, I. J., Borsato, A., Tooth, A. F., Frisia, S., Hawkesworth, C. J., Huang, Y. and  
750 Mcdermott, F.: Controls on trace element  $\delta$  Sr – Mg / compositions of carbonate cave  
751 waters : implications for speleothem climatic records, 2000.
- 752 Farrington, P., Turner, J. and Gailitis, V.: *Eucalyptus marginata*, *Trees*, 11, 9–15, 1996.
- 753 **Ford D. and P. D. Williams (1994) *Karst Hydrogeology and Geomorphology*, Wiley,**  
754 **Chichester.**
- 755 Genty, D. and Deflandre, G.: Drip flow variations under a stalactite of the Pere Noel cave  
756 (Belgium). Evidence of seasonal variations and air pressure constraints, *J. Hydrol.*, 211(1-4),  
757 208–232, doi:10.1016/S0022-1694(98)00235-2, 1998.
- 758 Gribovszki, Z., Szilágyi, J. and Kalicz, P.: Diurnal fluctuations in shallow groundwater levels  
759 and streamflow rates and their interpretation - A review, *J. Hydrol.*, 385(1-4), 371–383,  
760 doi:10.1016/j.jhydrol.2010.02.001, 2010.
- 761 Hartmann, a, Goldscheider, N., Wagener, T., Lange, J. and Weiler, M.: Karst water resources  
762 in a changing world: Approaches, of hydrological modeling, *Rev. Geophys.*, (1), 1–25,  
763 doi:10.1002/2013RG000443.Received, 2014a.
- 764 Hartmann, A., Mudarra, M., Andreo, B., Marin, A., Wagener, T. and Lange, J.: Modelling  
765 spatiotemporal impacts of hydroclimatic extremes on groundwater recharge at a  
766 Mediterranean karst aquifer, *Water Resour. Res.*, 50, 6507–6521,

767 doi:10.1002/2014WR015685.Received, 2014b.

768 Hartmann, A., Gleeson, T., Rosolem, R., Pianosi, F., Wada, Y. and Wagener, T.: A large-scale  
769 simulation model to assess karstic groundwater recharge over Europe and the  
770 Mediterranean, *Geosci. Model Dev.*, 8(6), 1729–1746, doi:10.5194/gmd-8-1729-2015, 2015.

771 Hu, C., Henderson, G. M., Huang, J., Chen, Z. and Johnson, K. R.: Report of a three-year  
772 monitoring programme at Heshang Cave, Central China, *Int. J. Speleol.*, 37(October), 143–  
773 151, doi:10.5038/1827-806X.37.3.1, 2008.

774 Jex, C. N., Mariethoz, G., Baker, A., Graham, P., Andersen, M. S., Acworth, I., Edwards, N.  
775 and Azcurra, C.: Spatially dense drip hydrological monitoring and infiltration behaviour at  
776 the Wellington Caves, South East Australia, *Int. J. Speleol.*, 41(2), 283–296, 2012.

777 Lange, J., Arbel, Y., Grodek, T. and Greenbaum, N.: Water percolation process studies in a  
778 Mediterranean karst area, *Hydrol. Process.*, 24(13), 1866–1879, doi:10.1002/hyp.7624,  
779 2010.

780 Mahmud, K., Mariethoz, G., Baker, a., Treble, P. C., Markowska, M. and McGuire, E.:  
781 Estimation of deep infiltration in unsaturated limestone environments using cave LiDAR and  
782 drip count data, *Hydrol. Earth Syst. Sci. Discuss.*, 12(9), 8891–8925, doi:10.5194/hessd-12-  
783 8891-2015, 2015.

784 Mariethoz, G., Baker, A., Sivakumar, B., Hartland, A. and Graham, P.: Chaos and irregularity  
785 in karst percolation, *Geophys. Res. Lett.*, 39(23), n/a–n/a, doi:10.1029/2012GL054270, 2012.

786 Markowska, M., Baker, A., Treble, P. C., Andersen, M. S., Hankin, S., Jex, C. N., Tadros, C. V.  
787 and Roach, R.: Unsaturated zone hydrology and cave drip discharge water response:  
788 Implications for speleothem paleoclimate record variability, *J. Hydrol.*,  
789 doi:10.1016/j.jhydrol.2014.12.044, 2015.

790 McDonald, J.: The 2002–2003 El Niño recorded in Australian cave drip waters: Implications  
791 for reconstructing rainfall histories using stalagmites, *Geophys. Res. Lett.*, 31(22),  
792 doi:10.1029/2004GL020859, 2004.

793 McDonald, J. and Drysdale, R.: Hydrology of cave drip waters at varying bedrock depths  
794 from a karst system in southeastern Australia, *Hydrol. Process.*, 1748(March), 1737–1748,  
795 doi:10.1002/hyp, 2007.

796 Merritt, M. L.: Estimating Hydraulic Properties of the Floridan Aquifer System by Analysis of  
797 Effects , Collier and Hendry Counties , Florida, Secretary, 70, 2004.

798 Meyer, K. W., Feng, W., Breecker, D. O., Banner, J. L. and Guilfoyle, A.: Interpretation of  
799 speleothem calcite  $\delta^{13}\text{C}$  variations: Evidence from monitoring soil  $\text{CO}_2$ , drip water, and  
800 modern speleothem calcite in central Texas, *Geochim. Cosmochim. Acta*, 142, 281–298,  
801 doi:10.1016/j.gca.2014.07.027, 2014.

802 Noronha, A. L., Johnson, K. R., Southon, J. R., Hu, C., Ruan, J. and McCabe-Glynn, S.:  
803 Radiocarbon evidence for decomposition of aged organic matter in the vadose zone as the  
804 main source of speleothem carbon, *Quat. Sci. Rev.*, 127, 37–47,  
805 doi:10.1016/j.quascirev.2015.05.021, 2015.

806 Peel, M. C., Finlayson, B. L. and McMahon, T. a.: Updated world map of the K oppen-Geiger  
807 climate classification, *Hydrol. Earth Syst. Sci. Discuss.*, 4, pp. 439–473, doi:10.5194/hess-11-  
808 1633-2007, 2007.

809 Proctor, C. J., Baker, a., Barnes, W. L. and Gilmour, M. a.: A thousand year speleothem  
810 proxy record of North Atlantic climate from Scotland, *Clim. Dyn.*, 16(10-11), 815–820,  
811 doi:10.1007/s003820000077, 2000.

812 Rau, G. C., Cuthbert, M. O., Andersen, M. S., Baker, A., Rutledge, H., Markowska, M., Roshan,  
813 H., Marjo, C. E., Graham, P. W. and Acworth, R. I.: Controls on cave drip water temperature  
814 and implications for speleothem-based paleoclimate reconstructions, *Quat. Sci. Rev.*, 127,  
815 1–18, doi:10.1016/j.quascirev.2015.03.026, 2015.

816 Rutledge, H., Baker, A., Marjo, C. E., Andersen, M. S., Graham, P. W., Cuthbert, M. O., Rau, G.  
817 C., Roshan, H., Markowska, M., Mariethoz, G. and Jex, C. N.: Dripwater organic matter and  
818 trace element geochemistry in a semi-arid karst environment: Implications for speleothem  
819 paleoclimatology, *Geochim. Cosmochim. Acta*, 135, 217–230,  
820 doi:10.1016/j.gca.2014.03.036, 2014.

821 Sheffer, N. a., Cohen, M., Morin, E., Grodek, T., Gimburg, A., Magal, E., Gvirtzman, H., Nied,  
822 M., Isele, D. and Frumkin, A.: Integrated cave drip monitoring for epikarst recharge  
823 estimation in a dry Mediterranean area, Sif Cave, Israel, *Hydrol. Process.*, 25(18), 2837–  
824 2845, doi:10.1002/hyp.8046, 2011.

825 Sondag, F., Van Ruymbeke, M., Soubiès, F., Santos, R., Somerhausen, A., Seidel, A. and  
826 Boggiani, P.: Monitoring present day climatic conditions in tropical caves using an  
827 Environmental Data Acquisition System (EDAS), *J. Hydrol.*, 273(1-4), 103–118,  
828 doi:10.1016/S0022-1694(02)00362-1, 2003.

829 Spate, A.: *Karst Values*, Hurstville., 2002.

830 Stern, H., Hoedt, G. de and Ernst, J.: Objective classification of Australian Climates, *Bur.*  
831 *Meteorol.* [online] Available from:  
832 [http://www.bom.gov.au/climate/environ/other/koppen\\_explain.shtml](http://www.bom.gov.au/climate/environ/other/koppen_explain.shtml) (Accessed 15  
833 October 2013), 2012.

834 Thakur, G., Brevdo, E., Fučkar, N. S. and Wu, H. T.: The Synchrosqueezing algorithm for time-  
835 varying spectral analysis: Robustness properties and new paleoclimate applications, *Signal*  
836 *Processing*, 93(5), 1079–1094, doi:10.1016/j.sigpro.2012.11.029, 2013.

837 Tooth, A. F. and Fairchild, I. J.: Soil and karst aquifer hydrological controls on the  
838 geochemical evolution of speleothem-forming drip waters, Crag Cave, southwest Ireland, *J.*  
839 *Hydrol.*, 273(1-4), 51–68, doi:10.1016/S0022-1694(02)00349-9, 2003.

840 Treble, P., Markowska, M., Tadros, C., Jex, C., Coleborn, K., Dredge, J., Baker, A., Roach, R.  
841 and Spate, A.: Reconstructing past environmental change at Yarrangobilly Caves, pp. 83–88.,  
842 2013a.

843 Treble, P. C., Bradley, C., Wood, A., Baker, A., Jex, C. N., Fairchild, I. J., Gagan, M. K., Cowley,  
844 J. and Azcurra, C.: An isotopic and modelling study of flow paths and storage in Quaternary  
845 calcarenite, SW Australia: implications for speleothem paleoclimate records, *Quat. Sci. Rev.*,

846 64, 90–103, doi:10.1016/j.quascirev.2012.12.015, 2013b.

847 Treble, P. C., Fairchild, I. J., Griffiths, A., Baker, A., Meredith, K. T., Wood, A. and McGuire, E.:  
848 Impacts of cave air ventilation and in-cave prior calcite precipitation on Golgotha Cave  
849 dripwater chemistry, southwest Australia, *Quat. Sci. Rev.*, 127,  
850 doi:10.1016/j.quascirev.2015.06.001, 2015.

851 Treble, P. C., Fairchild, I. J., Baker, A., Meredith, K. M., Andersen, M. S., Salmon, S. U.,  
852 Bradley, C., Wynn, P. M., Hankin, S., Wood, A. and McGuire, E.: Roles of bioproductivity,  
853 transpiration and fire in an eight-year record of cave dripwater chemistry from a forested  
854 catchment, southwest Australia, *Quat. Sci. Rev.*, [in press](#), 2016.

855 Tremaine, D. M. and Froelich, P. N.: Speleothem trace element signatures: A hydrologic  
856 geochemical study of modern cave dripwaters and farmed calcite, *Geochim. Cosmochim.*  
857 *Acta*, 121, 522–545, doi:10.1016/j.gca.2013.07.026, 2013.

858 Webb, M., Dredge, J., Barker, P. A., Müller, W., Jex, C., Desmarchelier, J., Hellstrom, J. and  
859 Wynn, P. M.: Quaternary climatic instability in south-east Australia from a multi-proxy  
860 speleothem record, *J. Quat. Sci.*, 29(6), 589–596, doi:10.1002/jqs.2734, 2014.

861 Wong, C. and Banner, J. L.: Response of cave air CO<sub>2</sub> and drip water to brush clearing in  
862 central Texas: Implications for recharge and soil CO<sub>2</sub> dynamics, *J. Geophys. Res.*, 115,  
863 doi:10.1029/2010JG001301, 2010.

864 Worboys, G.: Kosciusko National Park Geology and Geomorphology, National Parks and  
865 Wildlife Services, Sydney., 1982.

866 Zapater, M., Hossann, C., Bréda, N., Bréchet, C., Bonal, D. and Granier, A.: Evidence of  
867 hydraulic lift in a young beech and oak mixed forest using <sup>18</sup>O soil water  
868 labelling, *Trees - Struct. Funct.*, 25(5), 885–894, doi:10.1007/s00468-011-0563-9, 2011.

869